Supplemental Material

Reduced expression of phosphatase PTPN2 promotes pathogenic conversion of Tregs in autoimmunity

Mattias N.D. Svensson, Karen M. Doody, Benjamin J. Schmiedel, Sourya Bhattacharyya, Bharat Panwar, Florian Wiede, Shen Yang, Eugenio Santelli, Dennis J. Wu, Cristiano Sacchetti, Ravindra Gujar, Gregory Seumois, William B. Kiosses, Isabelle Aubry, Gisen Kim, Piotr Mydel, Shimon Sakaguchi, Mitchell Kronenberg, Tony Tiganis, Michel L. Tremblay, Ferhat Ay, Pandurangan Vijayanand and Nunzio Bottini*

*Corresponding author: Nunzio Bottini, MD, PhD, Department of Medicine, University of California San Diego ACTRI, 9452 Medical Center Dr., La Jolla, CA 92037, Phone: +1 (858) 246-2398, Email: nbottini@ucsd.edu

Supplemental material and methods

Mice

Generation of *Ptpn2*^{floxed} B6 mice has recently been described(1). Briefly, the targeting construct included two LoxP sites flanking exon 6, an IRES dependent Cerulean cassette and a neomycin resistance cassette, both of which are flanked by FRT sites. R1 ES cells were electroporated and correctly targeted clones were injected in B6 blastocysts. Chimeric mice were mated with B6 mice and subsequently backcrossed for eight generations to the B6 background. *Ptpn2*^{floxed} B6 were used at 6-8 weeks of age for further breeding with Cre mice unless otherwise noted.

BALB/c IFNγ-KO (JAX# 002286, C.129S7(B6)-*Ifng*^{tm1Ts}/J(2)) mice were obtained from Jackson laboratories and bred with SKG mice.

Animal models of arthritis

For the Collagen Antibody-Induced Arthritis model (CAIA), 8-week-old male BALB/c mice were injected with 2 mg of anti-collagen antibody cocktail i.p. (ArthritoMab™, MD Bioscience). After 3 days, mice were injected with 100 ug LPS i.p. (MD Bioscience) to boost induction of arthritis. Assessment of arthritis was performed as for the K/BxN serum transfer model.

For B cell depletion experiments, female SKG mice were injected with anti-mouse CD20 (100 μg) or isotype control (MOPC21) obtained from Biogen Idec, USA. Mice were treated by retro-orbital injection once a week starting 14 days after mannan injection. Mice were injected with mannan at 8 weeks of age.

All arthritis studies were performed on littermate mice. For B cell depleting mice with similar degree of arthritis was treated with wither B cell depleting or control antibodies. Clinical scoring of mice was performed in a blinded manner in which treatments were blinded to the researcher during scoring.

Assessment of inflammation with an intravital probe

The Xenolight Rediject Inflammation Probe (PerkinElmer) is an intravital luminescent dye that penetrates phagocytic cells and enables intravital assessment of joint inflammation. 3 days after K/BxN serum-induced arthritis induction, the probe was administered to mice by i.p. injection according to the manufacturer's instructions. Joint

inflammation was quantified using a Xenogen IVIS Spectrum in vivo imaging system (PerkinElmer).

Histological assessment of arthritic joints

Hind paws were fixed in 10% neutral-buffered formalin, decalcified, and embedded in paraffin. Sections were prepared from tissue blocks by HistoTox (Boulder, CO) and stained with H&E and safranin-O/Fast Green/Hematoxylin (Sigma-Aldrich). Histopathological scoring for inflammation, bone erosion, and cartilage erosion was performed in a blinded manner as previously described(3). Scoring of synovial inflammation, bone destruction and cartilage depletion was performed in a blinded manner by two independent researchers.

Micro-CT

Ankles were place in 10% neutral-buffered formalin. After fixation, samples were transferred to 70% ethanol. Before scanning, bones were transferred to PBS for 48 hours. Scanning was performed on a Skyscan1176 micro-CT (Bruker, Antwerp, Belgium) with a voxel size of 9 µm, at 50 kV/ 200 mA, with a 0.5 mm aluminum filter. Exposure time was 810 ms. The X-ray projections were obtained at 0.4° intervals with a scanning angular rotation of 180° and a combination of 4 average frames. The projection images were reconstructed into 3D images using NRECON software (Bruker) and CT-Analyzer (Bruker). Images were generated using the CT-VOX software (Bruker).

Gene-expression analysis

Arthritic ankles were flash frozen in liquid nitrogen and stored. RNA was isolated from arthritic ankles using TRIzol (Invitorgen) according to manufacturer's protocol.

For evaluation of gene expression in naïve ($CD4^+CD44^+CD62L^+FoxP3^-eGFP^-$), effector/memory ($CD4^+CD44^{hi}CD62L^-FoxP3^-eGFP^-$) and Tregs ($CD4^+FoxP3^+eGFP^+$), cells were sorted using flow cytometry from pre-arthritic (8-week-old) *Ptpn2*$^{+/+}$ and *Ptpn2*$^{+/-}$ male $FoxP3^{eGFP}$ SKG mice. After sorting cells were lysed in RLT buffer and RNA was isolated using the RNeasy Micro Kit (Qiagen) according to manufacturer's protocol. cDNA was synthesized using the SuperScript® III RT Kit (Thermo Fisher), according to the manufacturer's instructions. Primer assays used for *Il17a* (PPM03023A), *Tnf* (PPM03113G), *Blimp1/Prdm1* (PPM25183F), *Cxcl12* (PPM02965E), *Cxcl13* (PPM02947G), *Lta* (PPM03114A), *Ltb* (PPM03119A), *Bcl6* (PPM04965C), *Il1b*

(PPM03109F), *Il6* (PPM03015A), *Rankl/Tnfsf11* (PPM03047F), *gp130/Il6st* (PPM03123C), *Il6ra* (PPM03027F), *Ptpn2* (PPM35755C), *Il21* (PPM03761F), *Foxp3* (PPM05497F), *Rorc* (PPM25095A) *and Gapdh* (PPM02946E) were obtained from Qiagen. *Gapdh* was used as reference gene and the results are presented as a fold change compared to either the expression level in *Ptpn2*$^{+/+}$ SKG BALB/c samples with the ΔΔCq method or as fold change compared to the expression of *Gapdh.*

Immunofluorescent staining of whole mounts of ankle tissue samples

For visualization of ectopic lymphoid structures (ELS) in arthritic ankles, whole mounts of synovial tissue samples isolated from arthritic ankles of male *Ptpn2*$^{+/+}$ and *Ptpn2*$^{+/-}$ SKG BALB/c mice 30 days after mannan injection were fixed overnight in 4% PFA at room temp. After fixation samples were transferred into a buffer containing 2% FBS, 0.5% Saponin and 0.1% Sodium Azide in PBS. Pieces of synovial tissue was removed from fixed ankles and stained over night with antibodies directed against CD4 (RM4-5, eBioscience) and B220 (RA3-6B2, eBioscience) in the buffer mentioned above. Nuclear staining was performed with Hoechst and samples were mounted using ProLong Gold Antifade (Thermo Scientific). Z stacks of multipanelled images created from the whole mounted samples were captured using a 60x objective (using a 0.5 micron step size) on an Olympus FluoView FV10i laser scanning confocal microscope. Each panel of images were obtained at a 10% overlap between sequential image tiles and then stitched together as a multi-panel mega image using the FluoView-ASW version 4.2 software (Olympus, Inc.). The Mega images were further processed as maximum intensity projections for presentation in figure panels.

Cell preparation and flow cytometry

Single-cell suspensions were prepared from lymph nodes, spleen and thymus. For isolation of synovial cells, joints were collected and bone marrow cells were flushed out. Joints were rinsed with PBS and dissociated with Liberase TM (Roche) at 37°C. Cells were pre-incubated with Fc block (BD Pharmingen) before antibody staining. For surface staining, fluorophore-conjugated antibodies specific for CD4 (RM4-5), CD8 (53-6.7), TCRβ (H57-597), CD19 (ID3), CD45.2 (30F11), CD45.1 (A20), CD25 (PC65.1), CD69 (H1.2F3), CD5 (53-7.3), CD62L (MEL-14), ICOS (7E.17G9) and CD44 (IM7) were obtained from eBioscience/Thermo Fisher. CCR6 (140706) and Mouse Vβ TCR

screening panel (catalog 557004) was obtained from BD Bioscience. For intracellular cytokine staining, cells were incubated with 20 ng/mL Phorbol 12-myristate 13-acetate (PMA, Sigma Aldrich) and 1 μm Ionomycin (Sigma Aldrich) in the presence of Brefeldin A (1:1000 dilution, eBioscience/Thermo Fisher) for 5h at 37°. Intracellular staining was performed with the IC fixation buffer (eBioscience/Thermo Fisher) and permeabilization buffer (eBioscience/Thermo Fisher). For intracellular staining of transcription factors the FoxP3/Transcription Factor staining buffer set was used (eBioscience/Thermo Fisher). Antibodies recognizing FoxP3 (FJK-16s), RORγt (B2D), IL-17A (eBio17B7), IFNγ (XMG1.2), IL-6 (MP5-20F3) and TNFα (MP6-XT22) were obtained from eBioscience/Thermo Fisher. Dead cells were excluded from analysis by staining with Fixable Viability dye from eBioscience/Thermo Fisher.

For staining of phosphorylated proteins, stimulated cells were fixed by adding pre-warmed IC fixation buffer in a ratio of 1:1 and incubating at 37°C. Cells were permeabilized using ice-cold methanol and stained with antibodies directed against phosphorylated STAT3 (pY705; clone 4/P-STAT3) STAT1 (pY701; clone 4a) and STAT5 (pY694; clone 47/STAT5(pY694)) obtained from BD Bioscience.

Cells were analyzed on a BD LSR II, BD Fortessa, BD FACS Canto II (BD Biosciences) or a Bio-Rad ZE5 Cell Analyzer. Flow cytometry data was analyzed using FlowJo software (Tree Star, Inc.). Gating of cells was based on isotype control and fluorochrome minus one (FMO) staining when needed.

Cell preparation for phosflow

For evaluation of phosphorylation of STAT3 by phosflow, effector Tregs ($CD44^{hi}CD62L^{-}$, Supplemental Figure 8B) were sorted by flow cytometry from *Ptpn2*$^{+/+}$ *and Ptpn2*$^{+/-}$ 8-week-old female $FoxP3^{eGFP}$ SKG BALB/c mice. After sorting, cells were rested for 3h at 37°C and then stimulated with IL-6 (Biolegend, 5 ng/mL) for 15 minutes. Cells were fixed and stained as described above.

For evaluation of phosphorylation of STAT1 by phosflow, CD4 T cells were isolated from *Ptpn2*$^{+/+}$ *and Ptpn2*$^{+/-}$ 8-week-old male SKG BALB/c mice using the EasySep™ Mouse CD4 T Cell Enrichment Kit (Stem Cell Technologies). After isolation, cells were rested for 3h at 37°C and then stimulated with INFγ (eBiosience, 5 and 50 ng/mL) for 15 minutes. Cells were fixed and stained as described above.

For evaluation of phosphorylation of STAT5 by phosflow, naïve CD4 T cells were isolated from *Ptpn2*$^{+/+}$ *and Ptpn2*$^{+/-}$ 8-week-old male SKG BALB/c mice using the EasySep™ Mouse Naïve CD4 T Cell Isolation Kit (StemCell Technologies). To induce expression of CD25, cells were stimulated with plate bound anti-CD3 (2 ug/mL) and anti-CD28 (1 ug/mL) for 24h. After 24 h cells were washed and rested for 2h and then stimulated with IL-2 (R&D systems, 0.2 and 2 ng/mL) for 15 and 60 minutes. Cells were fixed and stained as described above.

In vitro Th differentiation

Naïve CD4 T cells were isolated from spleen and lymph nodes from *Ptpn2*$^{+/-}$ and *Ptpn2*$^{+/+}$ 8-week-old male SKG mice using the EasySep™ Mouse Naïve CD4 T Cell Isolation Kit (StemCell Technologies) and cultured under Th1 or Th17 polarizing conditions.

For differentiation of Th1 cells, naïve CD4 T cells were primed overnight with plate bound anti-CD3 (145-2C11, Biolegend, 2 μg/ml), soluble anti-CD28 (37.51, Biolegend, 0.5 μg/mL), anti-IL4 (11B11, Biolegend, 10 μg/mL) and recombinant IL-12 (R&D Systems, 25 ng/mL). After 24 hours, primed cells were re-stimulated with plate-bound anti-CD3 (2 μg/mL), anti-IL4 (10 μg/mL), IL-12 (25 ng/mL) and IL-2 (10 ng/mL) for 72h. After another 72h, cells were again re-stimulated with plate-bound anti-CD3 (2 μg/mL), anti-IL4 (10 μg/mL), IL-12 (25 ng/mL) and IL-2 (10 ng/mL) for 72h. To verify Th1 differentiation cells were stimulated with PMA (20 ng/mL) and ionomycin (1 μM) in the presence of Brefeldin A for 4h and analyzed by flow cytometry for expression of IFNγ.

For Th17 differentiation, naïve CD4 T cells were primed overnight with plate-bound anti-CD3 (2 μg/mL), soluble anti-CD28 (1 μg/mL), anti-IFNγ (XMG1.2, 10 μg/mL), anti-IL-4 (10 μg/mL), rhTGFβ1 (R&D Systems, 5 ng/mL) and IL-6 (Biolegend, 1 or 10 ng/mL). After priming, cells were restimulated with plate bound anti-CD3 (2 μg/mL), rhTGFβ1 (5 ng/mL) and IL-6 (1 or 10 ng/mL) for 72h. After 72h the cells were re-stimulated with plate bound anti-CD3 (2 μg/mL), rhTGFβ1 (5 ng/mL) and IL-6 (1, or 10 ng/mL) for 72h. To verify Th17 differentiation cells were stimulated with PMA (20 ng/mL) and ionomycin (1 μM) in the presence of Brefeldin A for 4h and analyzed by flow cytometry for expression of IL-17A.

In vitro upregulation of CD25 and CD69 in response to TCR stimulation

Naïve CD4 T cells were isolated from pooled spleen and lymph nodes of *Ptpn2*$^{+/+}$ and *Ptpn2*$^{+/-}$ male SKG BALB/c mice using the EasySep™ Mouse Naïve CD4 T Cell Isolation Kit (StemCell Technologies). Isolated cells were stimulated with varying concentrations of plate bound anti-CD3 together with soluble anti-CD28 (0.5 μg/mL) for different time points. Expression of CD69 and CD25 was evaluated by flow cytometry.

Treg suppression assay in vitro

Tregs (CD4^{+}FoxP3^{eGFP+}) were flow-sorted from spleen and lymph nodes of *Ptpn2*$^{+/+}$ and *Ptpn2*$^{+/-}$ 8-week-old female FoxP3^{eGFP} SKG BALB/c mice, whereas naïve CD4 T cells (CD4^{+}CD62L^{+}CD44^{low}CD25^{-}) were sorted from spleen of female *Ptpn2*$^{+/+}$ BALB/c mice. Naïve CD4 T cells were stained with CellTrace Violet (Invitrogen) to track proliferation. 5x10^{4} naïve T cells were plated together with varying numbers of Tregs. T cells were stimulated with 5 μg/mL of anti-CD3 (Biolegend) and 10x10^{4} irradiated splenocytes (3,500 rad) from female Rag2-KO mice as APCs. Cells were stimulated for 4 days after which proliferation and expression of CD25 on naïve CD4 T cells was evaluated by flow cytometry.

RNA-sequencing

RNA from sorted IL-17^{+} exTregs and Tregs was prepared using miRNeasy micro kit (Qiagen) and quantified as described previously(4, 5). RNA-Sequencing was performed as previously described. Briefly, 5 ng of purified total RNA was used for poly(A) mRNA selection(6). Purified total RNA (5 ng) was amplified following the Smart-seq2 protocol and amplified cDNA purified with AMPure XP beads (1:1 ratio; Beckman Coulter). 1 ng of cDNA was used for library preparation with using Nextera XT DNA sample preparation kit and index kit (Illumina, catalog# FC-131-1096). Samples were sequenced using a HiSeq2500 (Illumina) to obtain 50-bp single end reads. To reduce assay-to-assay variability, both whole transcriptome amplification and sequencing library preparations were performed in a 96-well format. Quality control steps were included to determine total RNA quality and quantity, the optimal number of PCR pre-amplification cycles, and fragment size selection (Bioanalyzer, Agilent), samples that failed quality control were eliminated from further downstream steps. Barcoded Illumina sequencing libraries were generated utilizing an ancillary automated platform (Biomek Fxp, Beckman

Coulter). Libraries were sequenced on the HiSeq2500 Illumina platform to obtain 50-bp single-end reads (HiSeq SBS and SR Cluster v4 kits, Illumine catalog# FC-401-4002 and GD-401-4001, respectively), generating an average of 11.4 million mapped reads / sample.

RNA-sequencing analysis

RNA-seq data were mapped against the separate mm10 reference genomes for C57BL_6J and BALB_cJ mice strains using TopHat (v2.0.9 (--max-multihits 1 --microexon-search --bowtie1) and the gene annotations downloaded from the Ensembl website. Trimmomatic (0.36) was used to remove adapters. The alignment results were parsed via the SAMtools to generate SAM files and read counts to each genomic feature were obtained with the htseq-count -m union -s no -t exon -i gene_name (part of the HTSeq framework, version 0.7.1). After removing absent features (zero counts in all samples), the raw counts were then imported to R/Bioconductor package DESeq2 (1.14.1) to identify differentially expressed genes among samples. The *P*-values for differential expression are calculated using binomial test for differences between the base means of two conditions. These p-values were then adjusted for multiple test correction using the Benjamini Hochberg algorithm to control the false discovery rate (FDR). We considered genes differentially expressed between two groups of samples when the DESeq2 analysis resulted in an adjusted *P*-value of <0.05 and the fold-change in gene expression > 2-fold.

MA-Plots, heat-maps and pathway analysis for RNA-Seq data

The ggmaplot function of ggpubr (v0.1.6) package for plotting MA-plots. Significantly up- and down-regulated genes are highlighted in the red and blue colors, respectively. Important genes are labeled in the box and all non-significant genes are shown in grey color. The heat-maps are generated using TPM (transcripts per million) values of differentially expressed genes in Qlucore Omics Explorer 3.2 software package. The TPM values are further converted into Z-score ranges from -2 to 2 (blue-to-yellow) for visualization purpose in heat-maps.

Pathway enrichments were calculated using the Ingenuity Pathway Analysis software (Qiagen). Up-regulated and down-regulated genes (comparing exTreg with

Tregs) with an adjusted *P*-value of <0.05 and a fold-change in gene expression > 2-fold were used for pathway analysis.

ATAC-Sequencing

ATAC-seq was performed according to Buenrostro *et al.*(7) with adoption of the improved Omni-ATAC protocol described by Corces *et al*(8). Briefly, live cells were lysed to extract nuclei in Omni-ATAC lysis buffer (10mM Tric-HCl pH 7.4, 10 mM NaCl, 3 mM $MgCl_2$, 0.1% NP-40, 0.1% Tween20 and 0.01% Digitonin). Nuclei were re-suspended in 50 μl Transposition mix (25 μl 2xTD buffer, 2.5 μL transposase [Nextera, Illumina], 16.5 μl PBS, 0.5 μl, 1% Digitonin, 0.5 μl, 10% Tween20 and 5 μl H2O) and the transposase reaction was conducted for 30 min at 37 °C. Right after tagmentation, fragments were purified by DNA precipitation and capture on columns (Zymo Research). Library amplification and barcoding were performed using Nextera DNA sample preparation kit and index kit (Illumina). Tagmented fragments were pre-amplified for 5 cycles followed by a second round of amplification based on the cell number (10 cycles for $0.5x10^5$ cells, 9 cycles for $1.0x10^5$ cells and 8 cycles for $1.5x10^5$ cells). Amplified libraries were purified using 1:1.8 ratio of Ampure XP Beads. Library fragments ranging in size, between 100 to 600bp, were size selected, using Ampure XP beads (ratios 1:0.5 and 1:1.8; Beckman Coulter). Libraries were quantified by Picogreen assay (Invitrogen) and size distribution was assessed using fragment analyzer (Advance Analytics). Single-end sequencing was performed on a HiSeq 2500 (Illumina) generating in total more than 250 millions 50 bp short sequencing reads (HiSeq SBS and SR Cluster v4 kits, Illumina catalog# FC-401-4002 and GD-401-4001, respectively). Raw data from the sequencer was demultiplexed and FASTQ files were generated using bcl2fastq conversion software (Illumina).

ATAC-Sequencing analysis

Single-end reads from ATAC-seq experiments were aligned to mm10 reference genome using Bowtie2 (version 2.3.3.1) (9, 10)], with parameters "*-k 4 --mm –threads 8 –X 2000"*. Reads corresponding to mitochondrial genome and chrY were filtered out. Uniquely mappable reads with mapping quality >= 30 were extracted using SAMtools (version 1.6)(11). Duplicate reads were removed by Picard tools MarkDuplicates (https://broadinstitute.github.io/picard). All reads aligning to the positive (+) strand were shifted by +4 bp, while all reads aligning to the negative (–) strand were shifted by -5 bp,

to account for the 9 bp distance between two adapters inserted by Tn5 transposase(7). Coverage tracks were normalized using "BamCoverage" from deepTools(12) with the arguments *"-bs 10 --effectiveGenomeSize 2652783500 --normalizeUsing RPKM -e 200"*. We used MACS2 (version 2.1.0)(13) for peak calling, with parameters: *"-g mm –q 0.05 --nomodel --nolambda --keep-dup all --call-summits --shift -100 --extsize 200"*. The summits of all peak were extended to regions with a uniform size of 500 bp. All of these uniform sized peaks were then merged to a global set of peaks, using bedtools merge routine(14). The number of transposase insertions for each of these uniform regions were computed with respect to individual samples, and normalized by their respective read counts(15). Differential ATAC-seq analysis was performed using DESeq2(16), and differentially accessible regions were filtered by FDR adjusted p-value of less than 0.05 and an estimated fold-change of at least 2. We used HOMER(17) to identify motifs for transcription factor binding sites enriched in different groups of peaks/regions. Motifs are declared as *significantly enriched* if the log p-value was less than -35, coverage above 10% and showed a fold increase of 2.5 over background coverage. Heat-map of -log p-values was generated by using Morpheus software (http://software.broadinstitute.org/morpheus). Heat maps show enrichment of transcription factors motifs in peaks enriched for a specific sample after pairwise comparison of Tregs 24h versus Tregs 48h (Treg 48h), Tregs 48h versus Tregs 72h (Treg 72h) and Tregs 72h versus exTregs 72h (exTreg 72h).

Analyses of DHS and overlap with RA-associated SNPs in *PTPN2* locus

In silico analysis of DHS sites in the human *PTPN2* locus and overlap with RA-associated SNPs were performed as previously described(18).To define the collection of RA-linked SNPs of the human *PTPN2* haploblock, we first checked for all RA-associated SNPs from the databases of GWAS Integrator(19) and HaploReg v3(20) (in April 2016), yielding a total of 3 significant lead SNPs ($P < 2 \times 10^{-8}$) in the *PTPN2* locus (rs2847297, rs1893217 and rs8083786). SNPs in tight genetic linkage ($r^2 > 0.8$) were retrieved based on data from the Phase I of the 1,000 Genome Project for all available reference populations (AFR, AMR, ASN and EUR; calculations performed using HaploReg v3; see Table S1). The total number of RA-associated SNPs located in the *PTPN2* locus on chromosome 18 was 79 (lead SNPs + linked SNPs).

To determine the number of DHS in the haploblock of the *PTPN2* locus, we downloaded genomic annotations of DHS from 113 cells types (primary cell types, fetal tissues and cell lines) provided by the ENCODE Project Consortium (ENCODE Encyclopedia, version 2; http://www.encodeproject.org(21)) and the NIH Epigenomics Roadmap Consortium (http://www.roadmapepigenomics.org(22)), and generated by the labs of Stamatoyannopoulos (Stam, University of Washington) and Crawford (Duke University). We utilized processed data provided by the ENCODE project; here the Stam lab merged all DNase peak data from the Stam and Crawford labs. This merging process formed one combined DNase-seq dataset with non-overlapping DHS. The Stam lab then identified the 'master' peak in each region, defined as the peak in the region with highest peak height/z-score. Utilizing this dataset, we found a total of 268 unique DHS in the *PTPN2* locus (chr18: 12,760,001-12,900,000 [hg19]; 140 kb).

Next, to determine the average number of DHS in the locus for each cell type, we merged replicates from cell types of similar origin (see details in Table S2). Of note, merged tracks of mixed or parental populations (*e.g.* data sets on 'CD3 cells' or 'CD4 primary cells') were excluded when data on subsets (such as 'CD4 naïve cells', 'T_H1 cells' and 'CD8 cells') were available. Our merged data set was used to determine the number of DHS within each cell type or tissue group of primary origin (shown in Figure 1B) and to identify DHS that intersect directly with RA-associated SNPs (shown in Figure 1C). The full list of merged DHS in primary cell types, including the number of single tracks for each cell type or tissue group, are provided in Table S3.

Immunoprecipitation and western blotting

Resting Tregs ($CD44^{low}CD62L^{+}$) were sorted by flow cytometry (Supplemental Figure 8B) from *Ptpn2*$^{+/+}$ and *Ptpn2*$^{+/-}$ 8 week-old female $FoxP3^{eGFP}$ SKG BALB/c mice and expanded in vitro with anti-CD3/CD28 coated beads (Invitrogen) and IL-2 (20 ng/mL). After expansion, cells were rested for 9h in complete RPMI Media (10% FBS, 1% L-Glutamine, 1% Penicillin/Streptomycin, 1% Non-Essential amino acids, 0.1% Beta-Mercaptoethanol), after which cells were stimulated with IL-6 (50 ng/mL) for 20 minutes. Stimulated cells were lysed and sonicated in ice cold 1xTNE buffer (50 mM Tris-HCl [pH 7.4], 150 mM NaCl, 5 mM EDTA, 1% NP-40, 1 mM PMSF) containing protease and phosphatase inhibitor cocktails (Roche). Lysates were pelleted and 5% was used as

whole lysate control. Lysates were pre-cleared with protein G sepharose beads (GE healthcare) for 30 minutes at 4°C, after which beads were removed and lysates incubated over night at 4°C with an anti-STAT3 antibody (79D7, Cell Signaling). STAT3 IP were captured using protein G sepharose beads. Membranes were blotted against phosphorylated STAT3 (pTyr705, D3A7, Cell Signaling), total STAT3 (79D7, Cell Signaling), PTPN2 (6F3, MediMabs) and GAPDH (14C10, Cell Signaling).

Bacterial expression and purification of proteins

Full-length human PTPN2 (amino acids 1-387) was subcloned into the NcoI-XhoI site of pET28a and expressed in *E. coli* strain BL21(DE3) as a C-terminal 6xHis tagged protein. Briefly, cultures were grown at 37°C to an OD600 of 0.7 with vigorous shaking and protein expression was induced with 0.2 mM isopropyl β-D-thiogalactopyranoside (IPTG) for 16-18 hours at 18°C. Following recovery from the soluble fraction of the cell lysate, the protein was purified by Nickel affinity (Ni-NTA, Qiagen) and size exclusion chromatography (ENrich™ SEC 650 10 x 300, Bio-rad), concentrated to 20 mg/ml and snap-frozen with 20 mM Tris, pH 7.3, 150 mM NaCl, 10 mM DTT as the final buffer. The substrate trapping mutant D182A, Q260A was designed on the basis of an analogous PTP1B mutant(23), generated by site-directed mutagenesis and purified the same way.

The plasmid encoding STAT3β(24) (a kind gift from Dr. Christoph Müller) was expressed in TKB1 (Agilent Technologies) and left unphosphorylated or phosphorylated according to the manufacturer's instructions. Untagged STAT3β pY705 (amino acids 127-722) was purified similar to PTPN2, except that the Nickel affinity step was replaced with ammonium phosphate precipitation as previously reported(24). Phosphorylation was confirmed by its smaller size exclusion retention volume compared to the unphosphorylated protein at similar concentrations, consistent with the formation of a dimer, and its reactivity towards an anti Phospho-STAT3 Antibody (pY705, D3A7, Cell Signaling Technology).

In vitro dephosphorylation assay of Stat3b

STAT3β pY705 was incubated at 5 nM concentration in a buffer containing 20 mM Tris pH 7.3, 50 mM NaCl, 10 mM DTT, 0.1% Triton X-100, in the presence or absence of an equal concentration of PTPN2. Samples were taken at 0, 1h45', 3h30' and 7h for analysis on SDS-PAGE followed by Western blot (anti-STAT3 pY705, Antibody D3A7,

Cell Signaling Technology). All samples were separated on a single 4-20% polyacrylamide gel.

In vitro substrate trapping

For in vitro substrate trapping, 10 µl of Ni-NTA beads (Qiagen) loaded with 10 µg PTPN2 substrate trapping mutant (D182A, Q260A) were incubated with 10 µg pY705 STAT3β for 1 hour at 4℃ and 1 hour at room temperature in total 90 µl of a buffer containing 20 mM Tris pH 7.3, 50 mM NaCl, 1 mM DTT, 0.01% Triton X-100. Unbound protein was removed by centrifugation and washed extensively with the same buffer in a micro spin column (Pierce). Proteins were eluted with 0.5 M imidazole pH 8.0 and analyzed by SDS-PAGE. Unphosphorylated STAT3β was used as a negative control.

Supplemental Figure 1

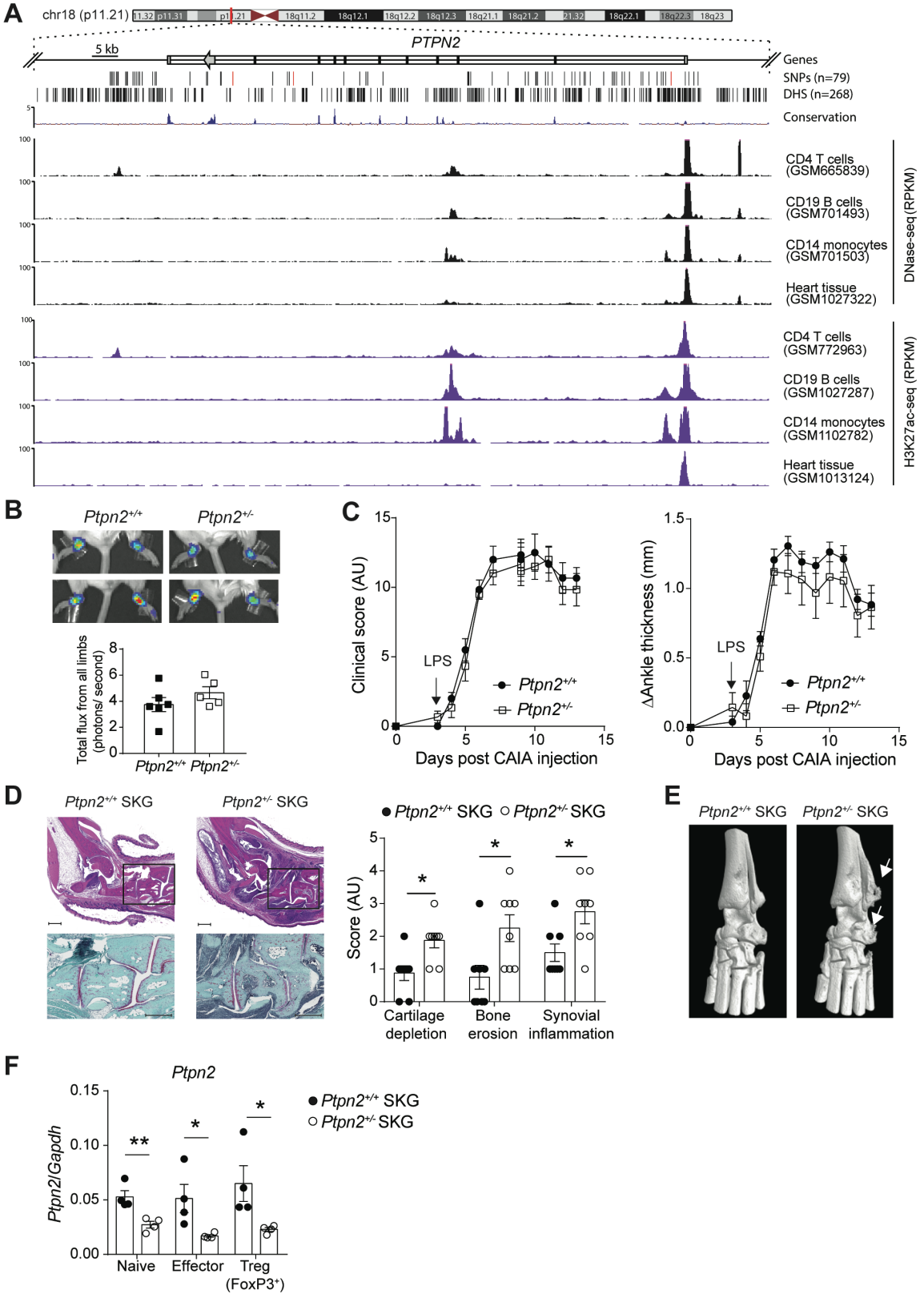

Supplemental Figure 1. RA-associated loss-of-function mutations in *Ptpn2* promote arthritis in SKG mice. A) University of California Santa Cruz (UCSC) tracks showing the chromosomal location of the human *PTPN2* gene body and locus, containing a large haplotype block of RA-associated SNPs. Black lines indicate SNPs' genomic location (the characterizing SNPs rs2847297, rs1893217 and rs8083786 are indicated in red), and DNase hypersensitivity sites (DHS) from multiple cell types obtained from the ENCODE Encyclopedia (version 2) provided by the ENCODE Project Consortium (see Methods). Exemplary tracks for DNase-I-hypersensitivity and histone modification H3K27ac in CD4 T cells, CD19 B cells, CD14 monocytes and heart tissue -provided by the ENCODE Project and NIH Epigenomics Roadmap Consortiums - are shown along with UCSC multispecies conservation tracks. **B**) Ankle luminescence (*top panel*) and ankle luminescence counts (*lower panel*) of male BALB/c mice on day 3 after arthritis induction with K/BxN serum ($Ptpn2^{+/+}$ n=6; $Ptpn2^{+/-}$ n=5). **C**) Clinical scores (*left panel*) and change in ankle thickness (*right panel*) during collagen antibody-induced arthritis (CAIA) in $Ptpn2^{+/+}$ (n=6) and $Ptpn2^{+/-}$ (n=6) male BALB/c mice. **D)** Representative hematoxylin/eosin (*left upper panels*) and safranin-O (*left lower panels*) images used for histological scoring of synovial inflammation, bone erosion and cartilage depletion in arthritic ankles of 20-25 weeks old female $Ptpn2^{+/+}$ (n=8) and $Ptpn2^{+/-}$ (n=8) SKG mice. Scoring quantification is shown in *right panel*. **E)** Representative micro-CT image of arthritic ankles from female $Ptpn2^{+/+}$ and $Ptpn2^{+/-}$ SKG with spontaneous arthritis. White arrows indicate bone erosion or reactive bone deposition. **F)** Expression of *Ptpn2* in naïve ($CD4^{+}CD62L^{+}CD44^{low}FoxP3^{eGFP-}$), effector ($CD4^{+}CD62L^{-}CD44^{hi}FoxP3^{eGFP-}$) and Tregs ($CD4^{+}FoxP3^{eGFP+}$) T cells sorted from $Ptpn2^{+/+}$ (n=4) and $Ptpn2^{+/-}$ (n=4) $FoxP3^{eGFP}$ SKG mice. Compiled data from at least two experiments are presented in (**B-F**). Bars represent mean ± SEM. $*P < 0.05$, $**P < 0.01$. $***P < 0.001$ by Mann-Whitney (**D**) or unpaired t-test (**F**).

Supplemental Figure 2

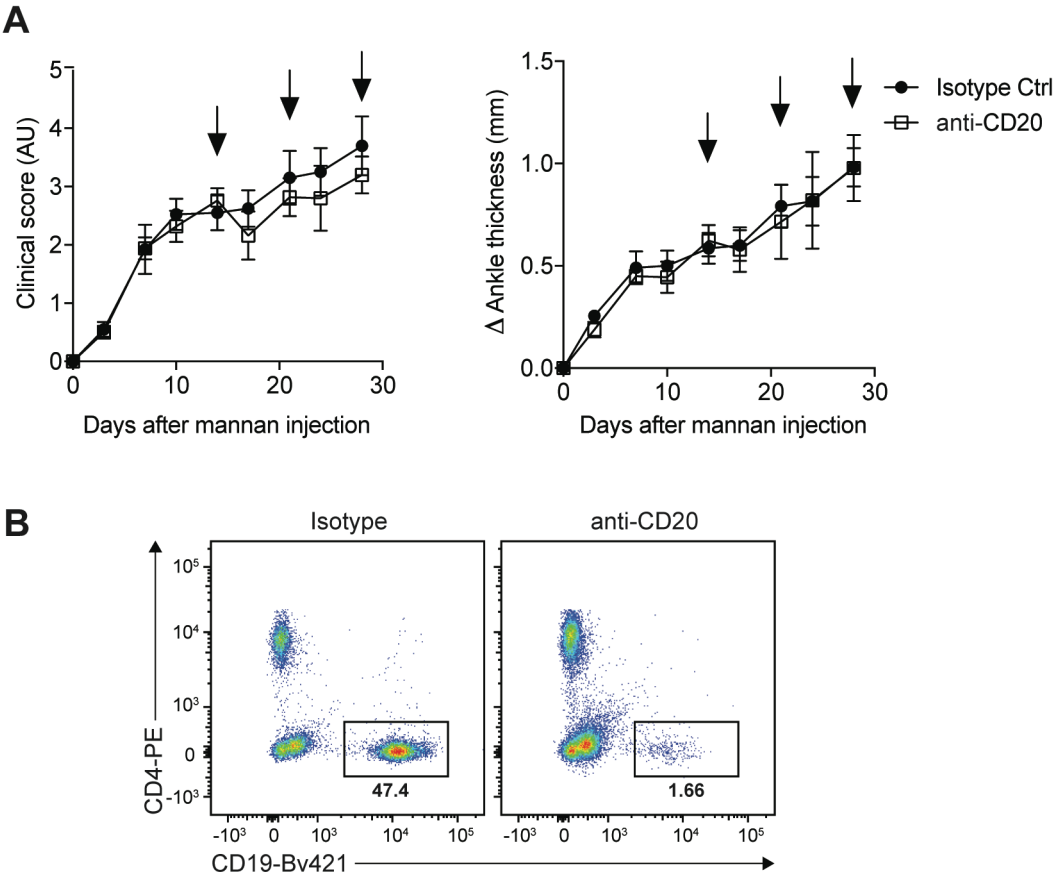

Supplemental Figure 2. B cells do not play a significant role in the effector phase of mannan-induced arthritis in SKG mice. Female SKG mice were treated with B cell-depleting anti-CD20 antibody (n=5) or isotype control (n=4) starting at day 14 after mannan injection (indicated by arrow). **A)** Clinical scores (*left panel*) and change in ankle thickness (*right panel*) after injection of mannan. **B)** Representative image of the frequency of CD19 B cells in peripheral blood in mice treated with either isotype or anti-CD20 antibodies. Bars represent mean ± SEM. Compiled data from three independent experiments are presented in (**A**).

Supplemental Figure 3

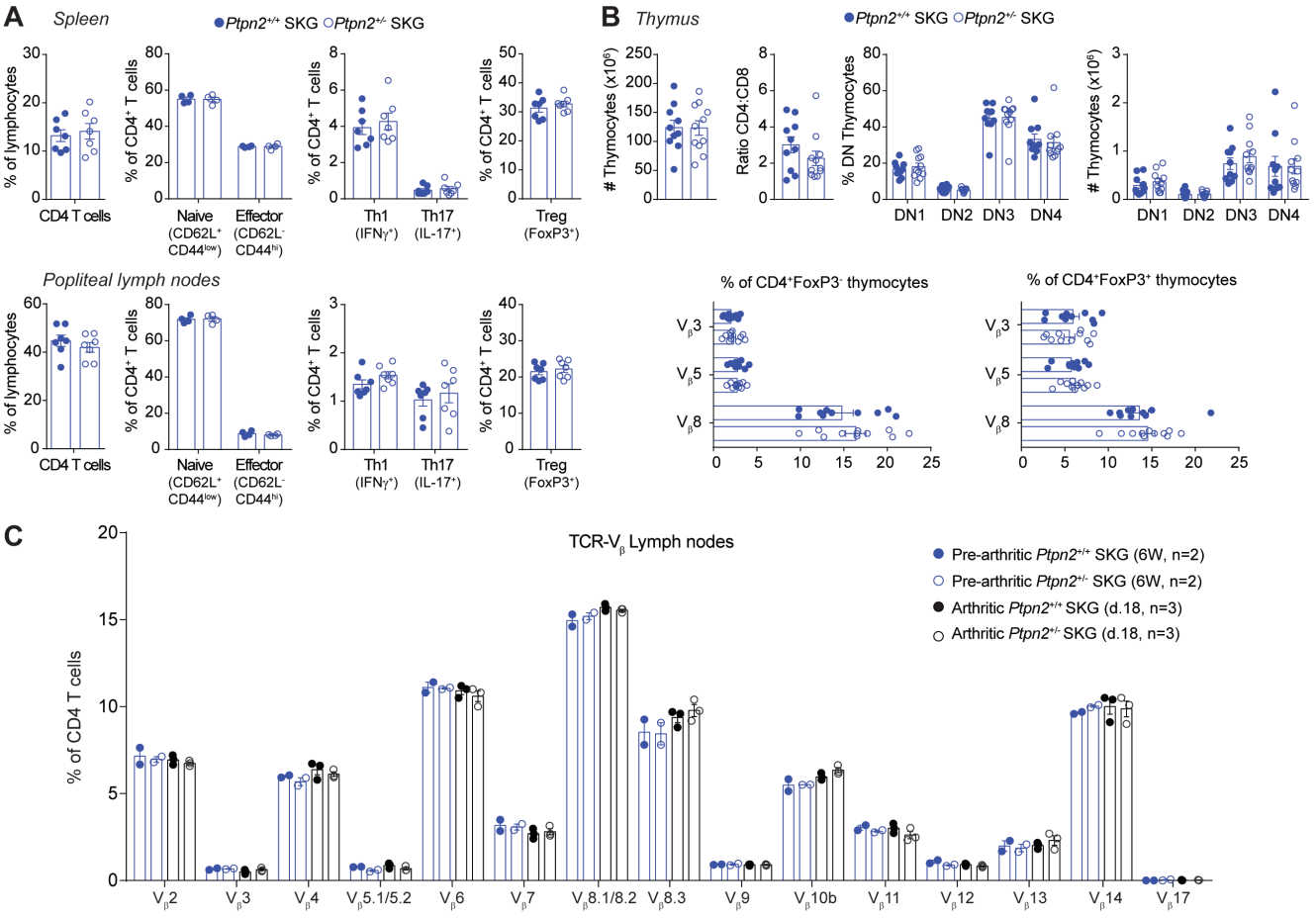

Supplemental Figure 3. *Ptpn2* haploinsufficient SKG mice show no alteration in naïve and effector CD4 T cells in the pre-arthritic phase, in thymic selection or in the frequency of CD4 T cell clones during arthritis. A) Frequency of total CD4 T cells and sub populations in the spleen (*upper panels*) and lymph nodes (*lower panels*) isolated from 8-week-old male *Ptpn2*$^{+/+}$ (n=7; for naïve and effector n=4) and *Ptpn2*$^{+/-}$ (n=7; for naïve and effector n=4) SKG mice. **B)** Evaluation of thymic development in 6-week-old male *Ptpn2*$^{+/+}$ (n=10) and *Ptpn2*$^{+/-}$ (n=11) SKG mice by flow cytometry. **C)** TCR V_β repertoire of CD4 SKG T cells analyzed in lymph nodes of pre-arthritic (6-week-old, n=2 per genotype) and arthritic (day 18 after mannan injection, n=3 per genotype) female *Ptpn2*$^{+/+}$ and *Ptpn2*$^{+/-}$ SKG mice by flow cytometry. Bars represent mean ± SEM. Compiled data from two independent experiments is presented in (**A-C**).

Supplemental Figure 4

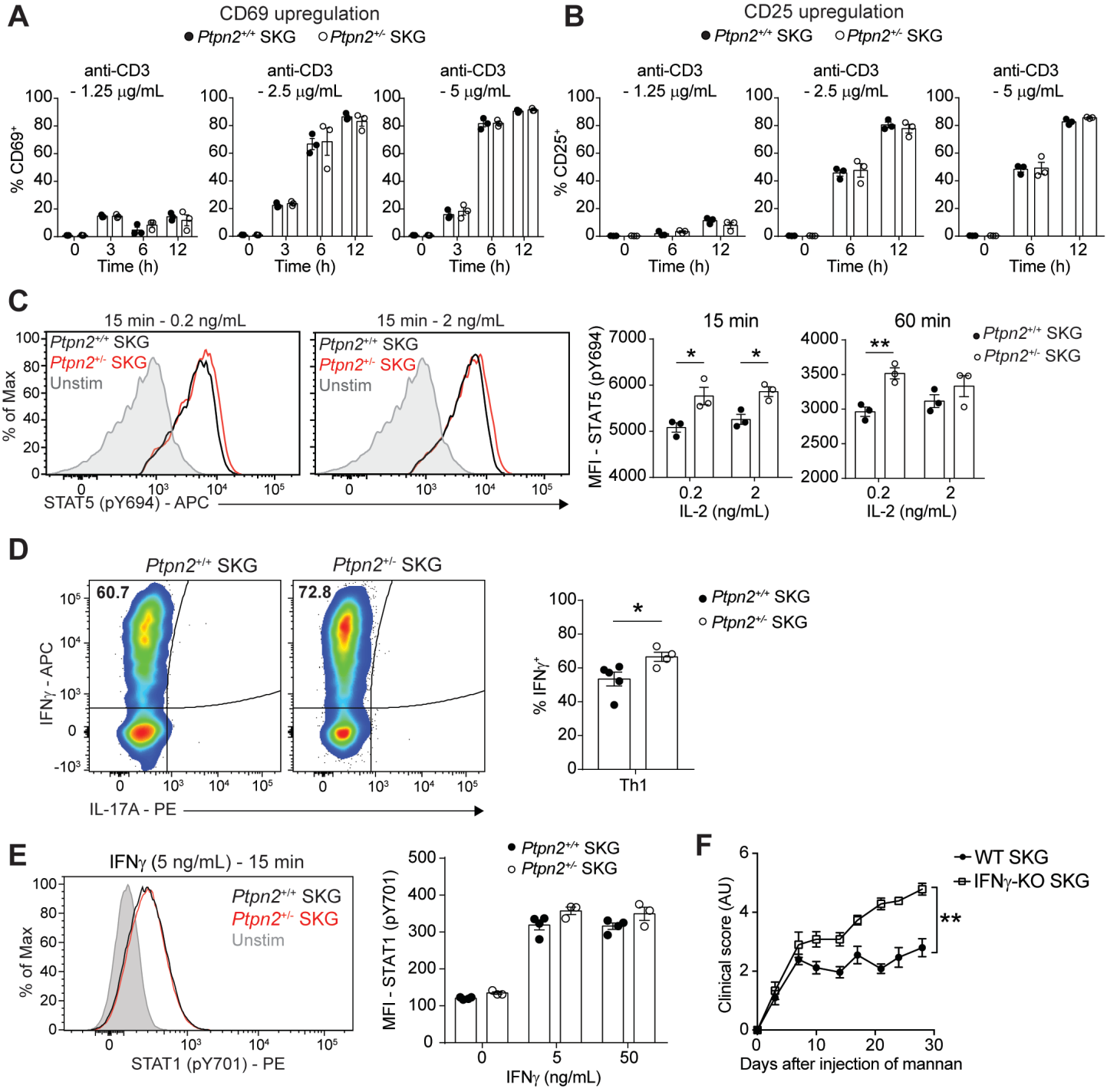

Supplemental Figure 4. *Ptpn2* haploinsufficiency promotes IL-2 signaling and Th1 polarization. A-B) Induction of CD69 (**A**) and CD25 (**B**) on *Ptpn2*$^{+/+}$ (n=3) and *Ptpn2*$^{+/-}$ (n=3) naïve CD4 SKG T cells after stimulation with anti-CD3 and anti-CD28. **C)** IL-2 induced induction of STAT5 (pY694) in naïve *Ptpn2*$^{+/+}$ (n=3) and *Ptpn2*$^{+/-}$ (n=3) CD4 SKG T cells. *Left panels* show representative flow histograms for 15 min stimulations. **D)** In vitro Th1 polarization from naïve *Ptpn2*$^{+/+}$ (n=5) and *Ptpn2*$^{+/-}$ (n=4) CD4 SKG T cells. *Left panels* show representative flow plots. **E**) Induction of STAT1 (pY701) analyzed by flow cytometry after IFNγ stimulation of CD4 T cells isolated from *Ptpn2*$^{+/+}$ (n=4) and *Ptpn2*$^{+/-}$ (n=3) SKG mice. *Left panel* shows representative flow histograms for 5 ng/mL IFNγ stimulation. **F)** Clinical scores of male IFNγ-KO (n=6) and WT (n=6) SKG mice after injection of mannan. Each symbol (**A-E**) represents an individual mouse. Compiled data from at least two individual experiments are presented in **(A, B, D, F)**. Data in **C** and **E** are representative of two independent experiments. Arthritis severity was quantified utilizing the area under the curve. Bars represent mean ± SEM. **P* < 0.05, ***P* < 0.01 by unpaired t-test **(C, D)** or by Mann-Whitney **(F).**

Supplemental Figure 5

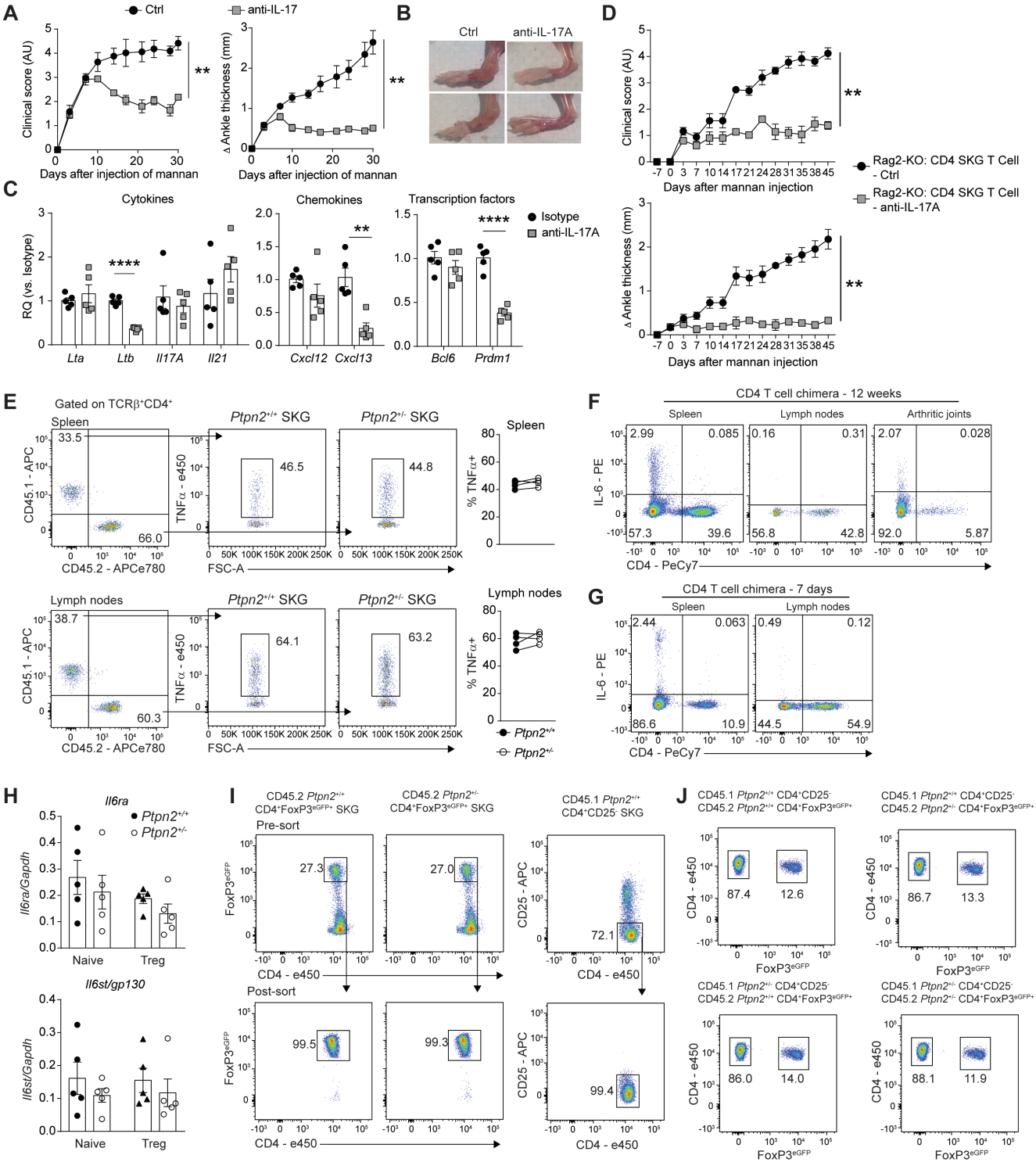

Supplemental Figure 5. Enhanced IL-17-dependent arthritis in *Ptpn2* haploinsufficient mice is not mediated through increased production of TNF and IL-6 or enhanced expression of IL-6R. A) Clinical scores (*left panel*) and change in ankle thickness (*right panel*) in female SKG mice treated with either anti-IL-17A (100 μg, n=5) or isotype control (n=5) antibodies weekly starting at the day of mannan injection. **B)** Representative images of arthritic ankles of mice in **A**. **C)** Expression of genes associated with ELS formation in arthritic ankles from mice in **A**. Data are presented as the relative quantification (RQ) compared to expression in control-treated SKG mice. **D)** Clinical score (*upper panel*) and change in ankle thickness (*lower panel*) of female Rag2-KO mice treated with anti-IL-17A after transfer of CD4 SKG T cells. One week after transfer, Rag2-KO mice were injected with mannan to induce arthritis. Starting at the day of mannan injection mice were treated with either anti-IL-17A antibody (100 μg, n=5) or isotype control (n=5). **E**) CD45.1 and CD45.2 CD4 T cells isolated from *Ptpn2*$^{+/+}$ or *Ptpn2*$^{+/-}$ male SKG mice were co-transferred into male Rag2-KO mice (n=4). One week after transfer, production of TNFα from CD4 T cells was assessed in spleen (*upper panels*) and lymph nodes (*lower panels*) by flow cytometry. *Left panels* show representative flow plots. **F-G)** Representative flow plots of production of IL-6 in spleen, lymph nodes and arthritic joints 7 days **(F,** n=4**)** and 11 weeks **(G,** n=3**)** after co-transfer of CD45.1 and CD45.2 CD4 T cells isolated from *Ptpn2*$^{+/+}$ and *Ptpn2*$^{+/-}$ male SKG BALB/c mice into male Rag2-KO mice. **H)** mRNA expression of *Il6ra* and *Il6st/gp130* in naïve ($CD4^+CD62L^+CD44^{low}FoxP3^{eGFP-}$), and Tregs ($CD4^+FoxP3^{eGFP+}$) T cells sorted from *Ptpn2*$^{+/+}$ (n=5) and *Ptpn2*$^{+/-}$ (n=5) $FoxP3^{eGFP}$ SKG mice. **I)** Flow sorting strategy and representative post sorting purity of Tregs ($CD4^+FoxP3^{eGFP+)}$ and CD25 negative CD4 T cells ($CD4^+CD25^-$) used for in vitro conversion assays, transfers to Rag2-KO mice and in vitro suppression assay. **J)** Distribution of $CD45.1^+CD4^+CD25^-$ (*Ptpn2*$^{+/+}$ *top panels* and *Ptpn2*$^{+/-}$ *lower panels*) and $CD45.2^+$ Tregs ($CD4^+FoxP3^{eGFP+,}$ *Ptpn2*$^{+/+}$ *left panels* and *Ptpn2*$^{+/-}$ *right panels*) injected into Rag2-KO mice. Experiments in (**E-F)** were performed once. Representative of two independent experiments are shown in (**A, C**). Compiled data from two independent experiments are shown in **(D, H).** Arthritis severity was quantified utilizing the area under the curve. Bars represent mean ± SEM. **P* < 0.05, ***P* < 0.01. ****P* < 0.001, *****P* < 0.0001 by for Mann-Whitney **(A-D)** or unpaired t-test **(C)**

Supplemental Figure 6

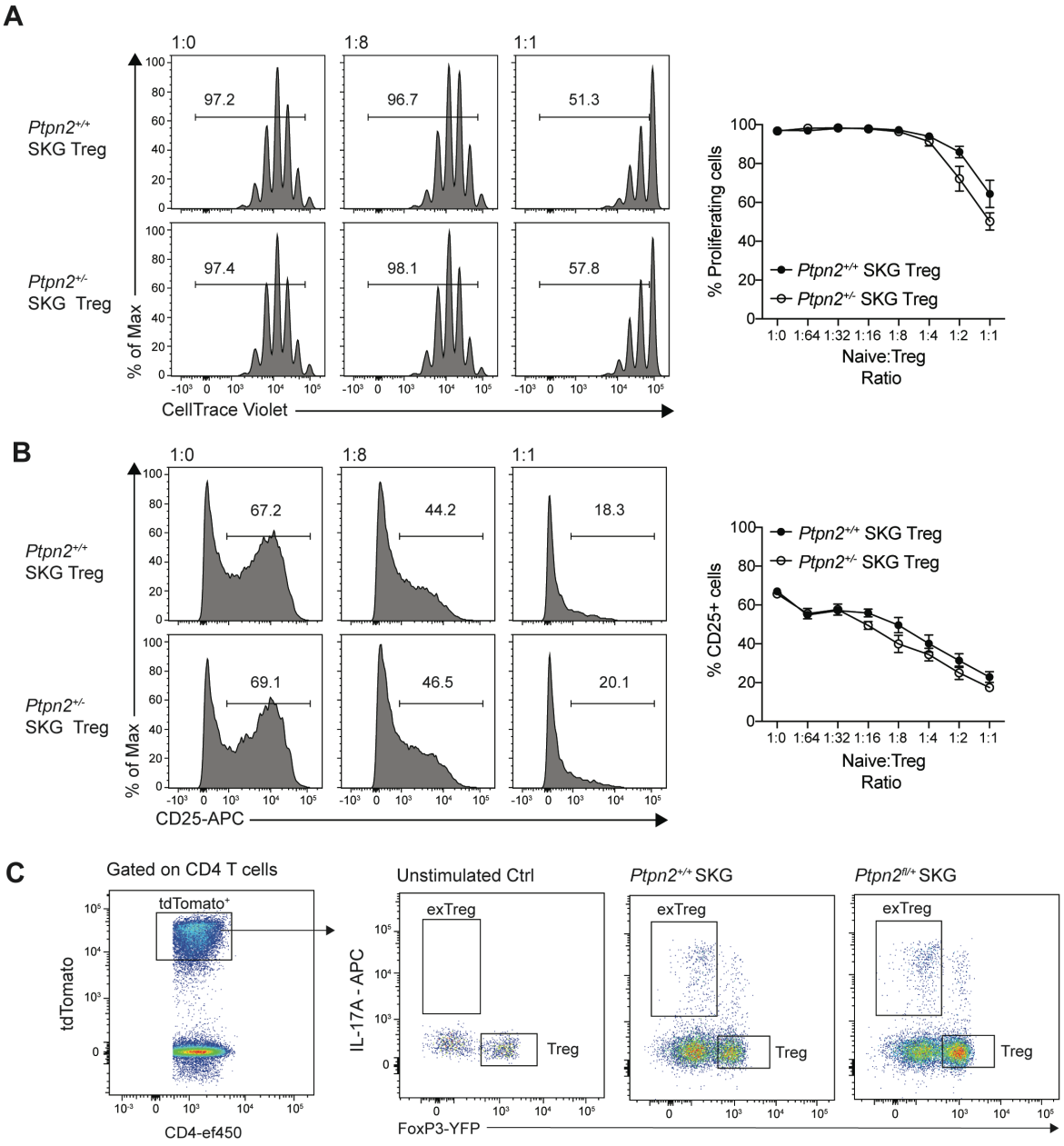

Supplemental Figure 6. Effect of *Ptpn2* haploinsufficiency for Treg function. A-B) In vitro Treg suppression assay using sorted CD45.2$^+$ naïve (CD4$^+$CD62L$^+$CD44^{low}CD25$^-$) BALB/c CD4 T cells and CD45.2$^+$ Tregs (CD4$^+$FoxP3^{eGFP+}) from *Ptpn2*$^{+/+}$ (n=3 individual mice) and *Ptpn2*$^{+/-}$ (n=3 individual mice) Foxp3^{eGFP} SKG mice. 5x10^4 naïve T cells and varying numbers of Tregs were stimulated for 4 days with 5 μg/mL soluble anti-CD3 and 1x10^5 irradiated Rag2-KO splenocytes as APCs. Proliferation (**A**) and expression of CD25

(**B**) was evaluated on CellTrace positive naïve BALB/c CD4 T cells using flow cytometry. *Left panels* show representative flow histograms. **C)** Gating strategy for sorting of IL-17A^{+} SKG exTregs and IL-17A^{-} SKG Tregs from B6.SKG.H2$^{d/d}$.FoxP3$^{YFP\text{-}cre+/-}$.tdTom$^{fl/+}$.*Ptpn2*$^{fl/+}$ fate mapping mice for RNA-seq. Results presented in (**A**) and (**B**) represents a single experiment. Bars represent mean ± SEM.

Supplemental Figure 7

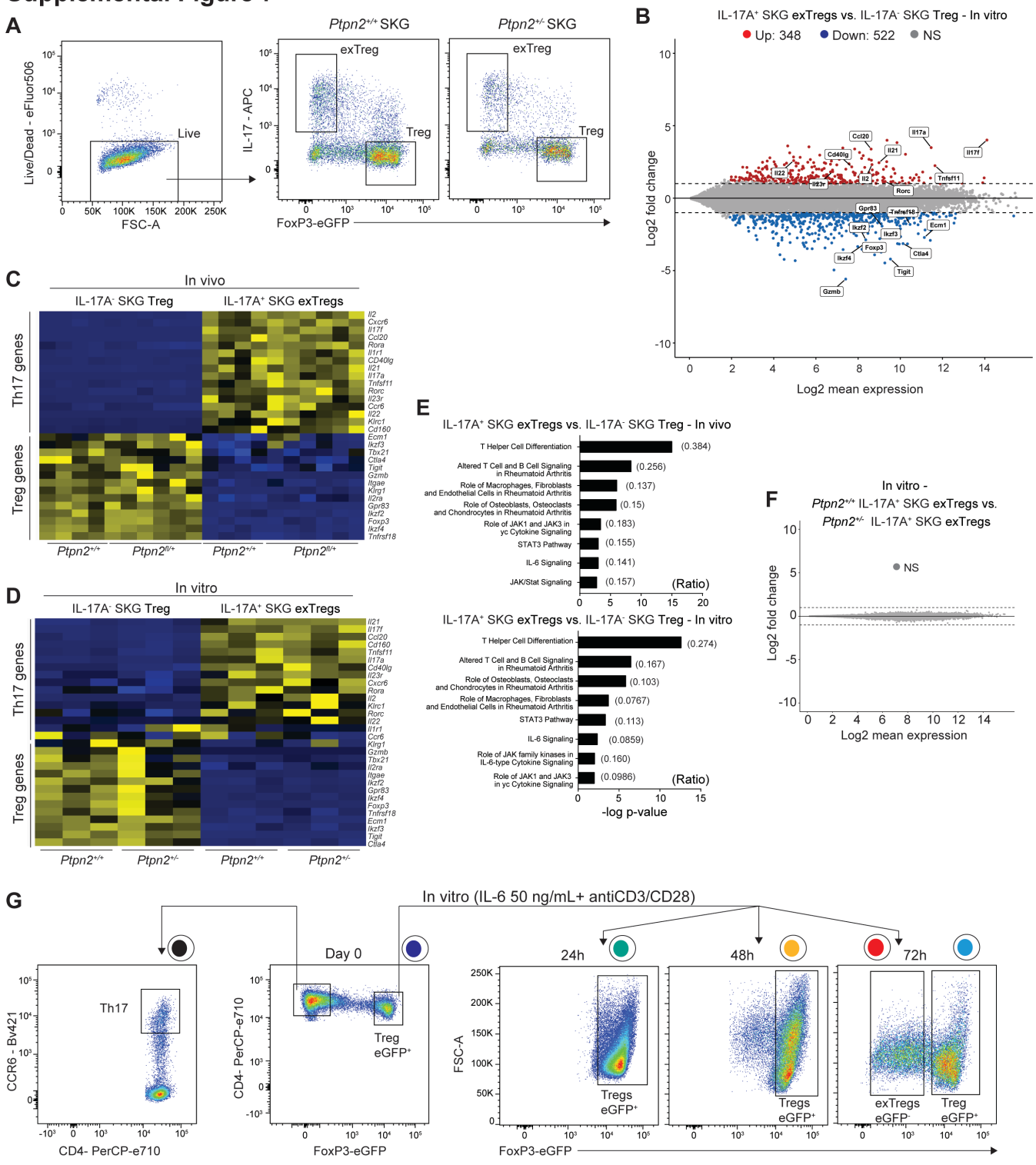

Supplemental Figure 7. Characterization of in vitro generated IL-17^{+} exTregs. A) Gating strategy for sorting of in vitro generated IL-17A^{+} SKG exTregs and IL-17A^{-} SKG Tregs for RNA-seq. **B-F**) RNA-Seq performed on IL-17^{+} SKG exTregs and IL-17^{-} SKG Tregs sorted from *Ptpn2*$^{fl/+}$ or *Ptpn2*$^{+/+}$ arthritic fate mapping mice or from in vitro conversion assay. **B**) MD-plot of significantly (*Padj* < 0.05 and fold change > 2) up-regulated (red) and down-regulated (blue) genes in IL-17A^{+} SKG exTregs vs. IL-17A^{-} SKG Tregs. **C-D**) Heat-map with 30 selected genes associated with Treg and Th17 differentiation program in IL-17^{+} SKG exTregs and IL-17^{-} SKG Tregs from fate mapping mice (**C**) or from in vitro conversion assay (**D**). Heat-map was generated with TPM values after normalization for transcript length. Genes with a fold change > 2 and *Padj* < 0.05 were used to generate the heat-map. **E**) Pathway analysis of differentially expressed genes in IL-17A^{+} SKG exTregs isolated from either fate mapping mice or from in vitro conversion assay. Generated using the Ingenuity Pathway Analysis software (Qiagen) using genes with a fold change > 2 and *Padj* < 0.05. **F**) MD-plot comparing *Ptpn2*$^{+/+}$ and *Ptpn2*$^{+/-}$ IL-17A^{+} SKG exTregs generated in vitro. **G)** Gating strategy for sorting of Th17 cells, Tregs and FoxP3^{+} Tregs and FoxP3^{-} exTregs during in vitro conversion for ATAC-seq analysis and for isolation of exTregs for transfer to Rag2-KO mice.

Supplemental Figure 8

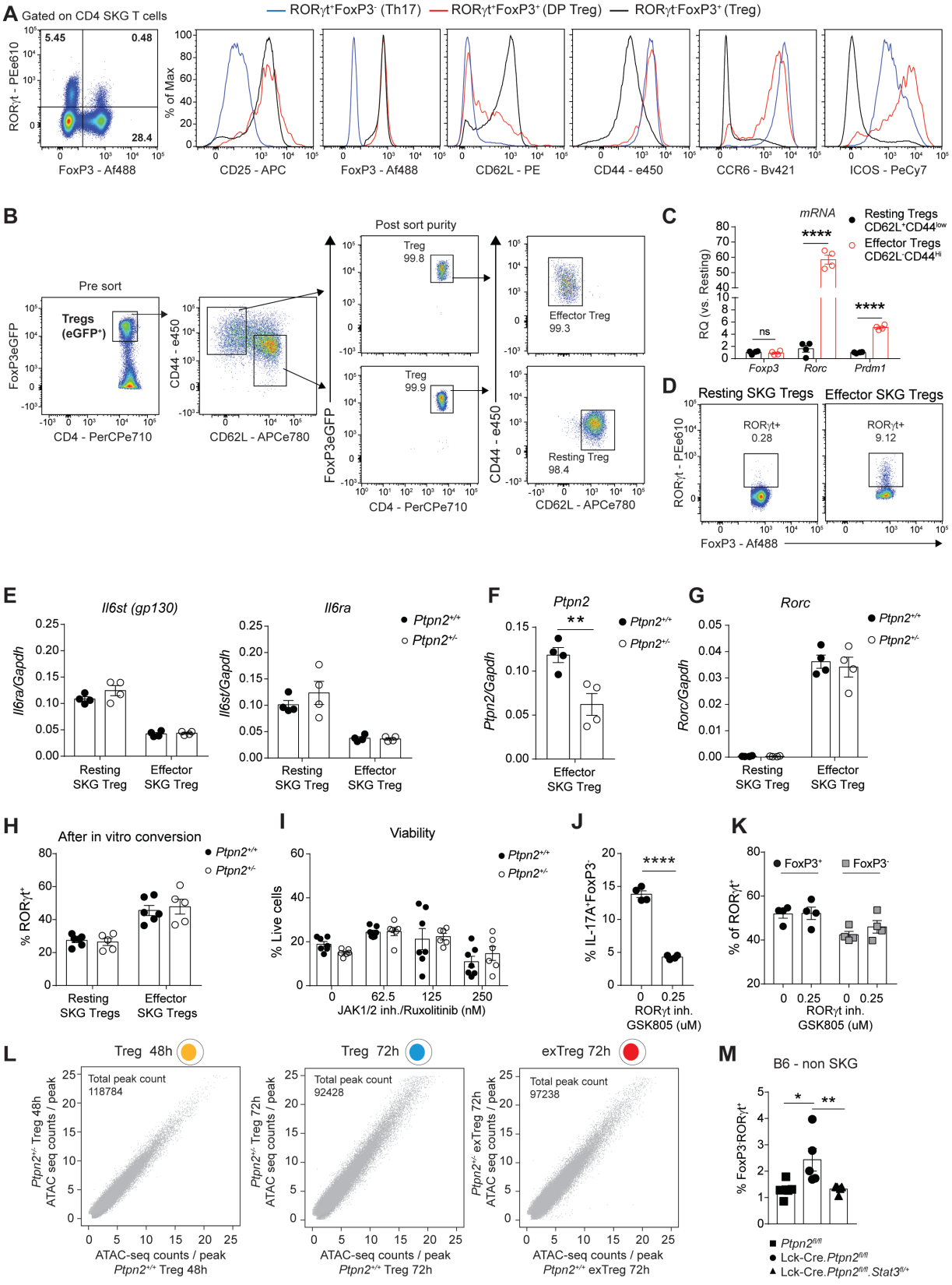

Supplemental Figure 8. In vitro conversion of effector Tregs is not mediated through the function of RORγt. A) Representative flow plot comparing the expression of selected markers on RORγt-expressing Tregs (RORγt^{+}FoxP3^{+}), Tregs (RORγt^{-}FoxP3^{+}) and Th17 cells (RORγt^{+}FoxP3^{-}) in joint draining lymph nodes (brachial, axillary and popliteal) of pre-arthritic female SKG mice (8-week-old). **B**) Gating strategy for flow cytometry based sorting of resting (CD4^{+}FoxP3^{eGFP+}CD62L^{+}CD44^{+}) and effector (CD4^{+}FoxP3^{eGFP+}CD62L^{-}CD44^{hi}) SKG Tregs and post sorting purity. **C**) Gene-expression of *Foxp3*, *Rorc* and *Prdm1* in sorted effector and resting Tregs from FoxP3^{eGFP} SKG mice (n=4). **D)** Representative frequency of RORγt-expressing cells within resting and effector SKG Tregs. Cells gated on effector and resting SKG Tregs as in (**B**). **E**) Expression of *Il6ra* and *Il6st (gp130)* in resting and effector SKG Tregs sorted as in (**B**) from pooled lymph nodes and spleen of *Ptpn2*$^{+/+}$ (n=4) or *Ptpn2*$^{+/-}$ (n=4) FoxP3^{eGFP} SKG mice. **F**) Expression of *Ptpn2* in effector SKG Tregs sorted as in (**B**) from lymph nodes of *Ptpn2*$^{+/+}$ (n=4) or *Ptpn2*$^{+/-}$ (n=4) FoxP3^{eGFP} SKG mice. **G**) Expression of *Rorc* in *Ptpn2*$^{+/+}$ (n=4) and *Ptpn2*$^{+/-}$ (n=4) resting and effector SKG Tregs (sorted as in **B**) before in vitro conversion. **H**) Expression of RORγt in *Ptpn2*$^{+/+}$ (n=5) and *Ptpn2*$^{+/-}$ (n=6) resting and effector SKG Tregs after 72h of in vitro conversion. **I**) Effect of JAK1/2 inhibition on the viability of *Ptpn2*$^{+/+}$ (n=7) and *Ptpn2*$^{+/-}$ (n=6) resting SKG Tregs after 72h of in vitro conversion. **J-K**) Effect of RORγt inhibition on generation of IL-17^{+} exTregs (**J**) and loss of FoxP3 from RORγt^{+} Tregs (**K**) during in vitro conversion of *Ptpn2*$^{+/+}$ SKG (n=4) Tregs. **L**) Comparison of the ATAC-signal per peak between *Ptpn2*$^{+/+}$ and *Ptpn2*$^{+/-}$ SKG Tregs during in vitro conversion. One replicate for each genotype is compared. **M**) FoxP3^{-}RORγt^{+} cells after in vitro conversion of *Ptpn2*$^{fl/fl}$ (n=5), Lck-Cre+*Ptpn2*$^{fl/fl}$ (n=5) and Lck-Cre+*Ptpn2*$^{fl/fl}$*Stat3*$^{fl/+}$ (n=5) Tregs isolated from non-SKG B6 mice. Compiled data from two independent experiments are shown in (**H, I).** Data in **(A-G, J, K)** are representative of at least two independent experiments. Symbols represents individual mice. Bars represent mean ± SEM. *P < 0.05, **P < 0.01, ****P < 0.0001 by unpaired t-test (**C**, **F**, **J**) or Mann-Whitney (**M**)

References for supplemental material

1. Bussieres-Marmen S, Vinette V, Gungabeesoon J, Aubry I, Perez-Quintero LA, and Tremblay ML. Loss of T-cell protein tyrosine phosphatase in the intestinal epithelium promotes local inflammation by increasing colonic stem cell proliferation. *Cell Mol Immunol.* 2017.
2. Dalton DK, Pitts-Meek S, Keshav S, Figari IS, Bradley A, and Stewart TA. Multiple defects of immune cell function in mice with disrupted interferon-gamma genes. *Science.* 1993;259(5102):1739-42.
3. Guma M, Ronacher L, Liu-Bryan R, Takai S, Karin M, and Corr M. Caspase 1-independent activation of interleukin-1beta in neutrophil-predominant inflammation. *Arthritis Rheum.* 2009;60(12):3642-50.
4. Seumois G, Vijayanand P, Eisley CJ, Omran N, Kalinke L, North M, Ganesan AP, Simpson LJ, Hunkapiller N, Moltzahn F, et al. An integrated nano-scale approach to profile miRNAs in limited clinical samples. *Am J Clin Exp Immunol.* 2012;1(2):70-89.
5. Seumois G, Chavez L, Gerasimova A, Lienhard M, Omran N, Kalinke L, Vedanayagam M, Ganesan AP, Chawla A, Djukanovic R, et al. Epigenomic analysis of primary human T cells reveals enhancers associated with TH2 memory cell differentiation and asthma susceptibility. *Nat Immunol.* 2014;15(8):777-88.
6. Picelli S, Faridani OR, Bjorklund AK, Winberg G, Sagasser S, and Sandberg R. Full-length RNA-seq from single cells using Smart-seq2. *Nat Protoc.* 2014;9(1):171-81.
7. Buenrostro JD, Giresi PG, Zaba LC, Chang HY, and Greenleaf WJ. Transposition of native chromatin for fast and sensitive epigenomic profiling of open chromatin, DNA-binding proteins and nucleosome position. *Nat Methods.* 2013;10(12):1213-8.
8. Corces MR, Trevino AE, Hamilton EG, Greenside PG, Sinnott-Armstrong NA, Vesuna S, Satpathy AT, Rubin AJ, Montine KS, Wu B, et al. An improved ATAC-seq protocol reduces background and enables interrogation of frozen tissues. *Nat Methods.* 2017;14(10):959-62.
9. Langmead B, Trapnell C, Pop M, and Salzberg SL. Ultrafast and memory-efficient alignment of short DNA sequences to the human genome. *Genome Biol.* 2009;10(3):R25.
10. Langmead B, and Salzberg SL. Fast gapped-read alignment with Bowtie 2. *Nat Methods.* 2012;9(4):357-9.
11. Li H, Handsaker B, Wysoker A, Fennell T, Ruan J, Homer N, Marth G, Abecasis G, Durbin R, and Genome Project Data Processing S. The Sequence Alignment/Map format and SAMtools. *Bioinformatics.* 2009;25(16):2078-9.
12. Ramirez F, Ryan DP, Gruning B, Bhardwaj V, Kilpert F, Richter AS, Heyne S, Dundar F, and Manke T. deepTools2: a next generation web server for deep-sequencing data analysis. *Nucleic Acids Res.* 2016;44(W1):W160-5.
13. Zhang Y, Liu T, Meyer CA, Eeckhoute J, Johnson DS, Bernstein BE, Nusbaum C, Myers RM, Brown M, Li W, et al. Model-based analysis of ChIP-Seq (MACS). *Genome Biol.* 2008;9(9):R137.
14. Quinlan AR, and Hall IM. BEDTools: a flexible suite of utilities for comparing genomic features. *Bioinformatics.* 2010;26(6):841-2.
15. Scott-Browne JP, Lopez-Moyado IF, Trifari S, Wong V, Chavez L, Rao A, and Pereira RM. Dynamic Changes in Chromatin Accessibility Occur in CD8(+) T Cells Responding to Viral Infection. *Immunity.* 2016;45(6):1327-40.

16. Love MI, Huber W, and Anders S. Moderated estimation of fold change and dispersion for RNA-seq data with DESeq2. *Genome Biol.* 2014;15(12):550.
17. Heinz S, Benner C, Spann N, Bertolino E, Lin YC, Laslo P, Cheng JX, Murre C, Singh H, and Glass CK. Simple combinations of lineage-determining transcription factors prime cis-regulatory elements required for macrophage and B cell identities. *Mol Cell.* 2010;38(4):576-89.
18. Schmiedel BJ, Seumois G, Samaniego-Castruita D, Cayford J, Schulten V, Chavez L, Ay F, Sette A, Peters B, and Vijayanand P. 17q21 asthma-risk variants switch CTCF binding and regulate IL-2 production by T cells. *Nat Commun.* 2016;7(13426.
19. Yu W, Yesupriya A, Wulf A, Hindorff LA, Dowling N, Khoury MJ, and Gwinn M. GWAS Integrator: a bioinformatics tool to explore human genetic associations reported in published genome-wide association studies. *Eur J Hum Genet.* 2011;19(10):1095-9.
20. Ward LD, and Kellis M. HaploReg: a resource for exploring chromatin states, conservation, and regulatory motif alterations within sets of genetically linked variants. *Nucleic Acids Res.* 2012;40(Database issue):D930-4.
21. Consortium EP. An integrated encyclopedia of DNA elements in the human genome. *Nature.* 2012;489(7414):57-74.
22. Bernstein BE, Stamatoyannopoulos JA, Costello JF, Ren B, Milosavljevic A, Meissner A, Kellis M, Marra MA, Beaudet AL, Ecker JR, et al. The NIH Roadmap Epigenomics Mapping Consortium. *Nat Biotechnol.* 2010;28(10):1045-8.
23. Xie L, Zhang YL, and Zhang ZY. Design and characterization of an improved protein tyrosine phosphatase substrate-trapping mutant. *Biochemistry.* 2002;41(12):4032-9.
24. Becker S, Corthals GL, Aebersold R, Groner B, and Muller CW. Expression of a tyrosine phosphorylated, DNA binding Stat3beta dimer in bacteria. *FEBS Lett.* 1998;441(1):141-7.

Table S1. GWAS-derived lead SNPs (highlighted in gray) and SNPs in tight genetic linkage.

Chromosome	Position (hg19)	Variant	Ref	Alt	AFR	AMR	ASN	EUR
18	12 774 326	rs2014857	C	T	0,81	0,86	0,84	0,85
18	12 774 639	rs34560559	GTA	G	0,11	0,11	0,16	0,13
18	12 774 894	rs888270	G	A	0,01	0,11	0,16	0,15
18	12 775 049	rs199624676	10-mer	G	0,08	0,11	0,14	0,14
18	12 775 050	rs142342883	11-mer	G	0,09	0,12	0,15	0,13
18	12 775 591	rs2847260	C	T	0,80	0,86	0,84	0,85
18	12 775 821	rs2847259	A	C	0,58	0,76	0,84	0,71
18	12 775 851	rs2542147	G	T	0,80	0,86	0,84	0,85
18	12 777 325	rs7237497	T	C	0,83	0,87	0,84	0,84
18	12 777 573	rs2542148	C	G	0,82	0,86	0,84	0,85
18	12 777 603	rs2847274	T	C	0,82	0,86	0,84	0,84
18	12 778 715	rs2847278	C	T	0,83	0,87	0,84	0,85
18	12 779 018	rs2542149	G	A	0,83	0,87	0,84	0,85
18	12 779 342	rs2847280	A	G	0,83	0,87	0,84	0,85
18	12 779 763	rs2542150	G	C	0,83	0,87	0,84	0,85
18	12 779 947	rs2542151	G	T	0,83	0,87	0,84	0,85
18	12 780 456	rs9952749	A	G	0,76	0,83	0,81	0,79
18	12 782 448	rs2847293	A	T	0,79	0,86	0,84	0,84
18	12 782 849	rs6505765	C	G	0,38	0,28	0,34	0,32
18	12 783 086	rs34920518	A	G	0,05	0,11	0,16	0,15
18	12 789 556	rs11663253	A	G	0,05	0,07	0,16	0,16
18	12 792 736	rs60474474	C	T	0,04	0,07	0,16	0,16
18	12 792 940	rs45450798	C	G	0,05	0,07	0,16	0,16
18	12 795 420	rs60751993	G	A	0,05	0,07	0,16	0,16
18	12 795 470	rs60735058	T	A	0,05	0,07	0,16	0,16
18	12 797 694	rs2847297	A	G	0,57	0,27	0,34	0,32
18	12 805 388	rs12967678	G	A	0,02	0,04	0,15	0,11
18	12 808 140	rs8096138	C	G	0,04	0,07	0,16	0,16
18	12 808 466	rs35153695	AC	A	0,04	0,07	0,16	0,16
18	12 809 340	rs1893217	A	G	0,05	0,07	0,16	0,16
18	12 812 896	rs2847288	C	G	0,48	0,81	0,83	0,83
18	12 818 922	rs80262450	G	A	0,01	0,03	0,14	0,11
18	12 821 903	rs16939895	G	A	0,21	0,11	0,37	0,15
18	12 823 056	rs547268	G	T	0,62	0,86	0,63	0,85
18	12 823 402	rs658158	T	G	0,60	0,86	0,64	0,85
18	12 826 385	rs8091566	G	A	0,61	0,85	0,63	0,85
18	12 842 480	rs12969241	G	T	0,01	0,04	0,16	0,11
18	12 842 567	rs35967540	G	C	0,01	0,04	0,16	0,11
18	12 842 681	rs35320197	C	A	0,01	0,04	0,16	0,11
18	12 843 137	rs11875687	T	C	0,20	0,10	0,32	0,15
18	12 847 136	rs657555	C	T	0,61	0,88	0,68	0,85
18	12 850 211	rs612058	T	C	0,62	0,88	0,68	0,86
18	12 853 458	rs487273	T	G	0,62	0,88	0,68	0,86
18	12 854 072	rs514000	C	T	0,38	0,84	0,64	0,85
18	12 855 440	rs484020	G	A	0,33	0,84	0,64	0,85
18	12 855 646	rs482160	A	G	0,55	0,86	0,64	0,85
18	12 855 864	rs34153303	G	A	0,01	0,04	0,16	0,11
18	12 857 335	rs534911	G	A	0,42	0,84	0,64	0,85
18	12 857 761	rs637643	C	T	0,45	0,89	0,84	0,96
18	12 858 610	rs579052	T	C	0,45	0,85	0,68	0,85
18	12 860 934	rs515151	G	C	0,62	0,88	0,68	0,85
18	12 862 395	rs683468	T	A	0,45	0,89	0,84	0,97
18	12 862 942	rs670671	A	C	0,45	0,89	0,84	0,97
18	12 863 840	rs34799913	T	G	0,01	0,04	0,16	0,11
18	12 864 674	rs507304	G	C	0,45	0,88	0,84	0,97
18	12 864 762	rs12955302	A	G	0,01	0,04	0,16	0,11
18	12 864 975	rs34735114	CAA	C	0,46	0,84	0,68	0,85
18	12 865 822	rs34416003	A	C	0,01	0,04	0,16	0,10
18	12 868 506	rs9959425	T	C	0,55	0,15	0,32	0,14

18	12 870 038	rs9959061	C	T	0,54	0,11	0,16	0,03
18	12 870 267	rs200065651	T	TAC	0,03	0,03	0,14	0,11
18	12 870 506	rs58509084	G	10-mer	0,46	0,15	0,28	0,12
18	12 870 510	rs58881251	T	7-mer	0,44	0,15	0,29	0,13
18	12 870 870	rs8091305	C	T	0,53	0,11	0,16	0,03
18	12 871 972	rs12964314	A	G	0,01	0,04	0,15	0,11
18	12 872 424	rs71353227	C	A	0,01	0,04	0,15	0,11
18	12 873 318	rs113404634	A	G	0,55	0,11	0,16	0,03
18	12 875 522	rs201079562	G	GT	0,55	0,15	0,31	0,15
18	12 875 975	rs34846641	A	G	0,58	0,15	0,32	0,15
18	12 877 060	rs7234029	A	G	0,57	0,15	0,32	0,15
18	12 878 582	rs12963474	C	A	0,01	0,04	0,16	0,11
18	12 879 466	rs12968719	G	A	0,01	0,04	0,16	0,11
18	12 879 737	rs8084365	T	A	0,56	0,12	0,16	0,04
18	12 880 206	rs7241016	A	G	0,57	0,15	0,32	0,15
18	12 881 361	rs8083786	A	G	0,57	0,15	0,32	0,15
18	12 883 939	rs9961931	A	C	0,56	0,12	0,16	0,03
18	12 884 676	rs8098730	A	T	0,56	0,12	0,16	0,03
18	12 885 577	rs35923716	A	G	0,01	0,04	0,15	0,11
18	12 886 441	rs35954636	T	G	0,01	0,03	0,15	0,11

Table S2. Analysis of publically available DNase-Seq datasets (ENCODE Project Consortium, see **Methods**), DNase hypersensitivity sites (DHS) in *PTPN2* locus in primary cell types (n=212), fetal tissues (n=279) and cell lines (n=107); in alphabetical order.

Cell type or tissue (group name)	Sample title (obtained from ENCODE master file)	DHS genome-wide	DHS in *PTPN2* locus **
Amniotic epithelial cells	HAEpiC-DS12663	258,482	19
Amniotic epithelial cells	HAEpiC-DS12673	253,993	19
Aortic adventitial fibroblasts	AoAF-DS13513	214,489	9
Aortic adventitial fibroblasts	AoAF-DS13523	224,168	13
Astrocytes	HAc-DS14765	231,197	14
Astrocytes	HAc-DS14770	194,994	11
Astrocytes	HAh-DS15192	259,294	15
Astrocytes	HAh-DS15202	231,377	15
Astrocytes	HAsp-DS14790	251,490	13
Astrocytes	HAsp-DS14794	225,989	14
Astrocytes	NHA-DS12800	246,721	13
Astrocytes	NHA-DS12805	206,072	13
B cells	CD19-DS17186	122,910	19
B cells	CD19-DS17281	111,460	12
B cells	CD19-DS17440	114,984	14
B cells	CD20-DS17371	222,477	17
B cells	CD20-DS17541	138,789	17
B cells	CD20-DS18208	131,909	14
Blood microvascular endothelial cells	HMVEC_dBlAd-DS13329	210,686	8
Blood microvascular endothelial cells	HMVEC_dBlAd-DS13337	205,904	9
Blood microvascular endothelial cells	HMVEC_dLyAd-DS13256	170,685	12
Blood microvascular endothelial cells	HMVEC_dLyAd-DS13261	162,792	11
Blood microvascular endothelial cells	HMVEC_dNeo-DS12929	186,986	10
Blood microvascular endothelial cells	HMVEC_dNeo-DS12937	180,984	9
Blood microvascular endothelial cells (lung derived)	HMVEC_LBl-DS13372	216,243	7
Blood microvascular endothelial cells (lung derived)	HMVEC_LBl-DS13375	198,617	7
Brain microvascular endothelial cells	HBMEC-DS13806	217,766	12
Brain microvascular endothelial cells	HBMEC-DS13817	254,940	10
Brain vascular pericytes	HBVP-DS14834	264,939	21
Brain vascular smooth muscle cells	HBVSMC-DS14845	208,588	22
Brain vascular smooth muscle cells	HBVSMC-DS14860	207,383	22
Bronchial epithelial cells (BEC)	NHBE_RA-DS11959	206,052	22
Bronchial epithelial cells (BEC)	NHBE_RA-DS11969	191,959	20
Cardiac fibroblasts	HCF-DS12491	216,472	13
Cardiac fibroblasts	HCF-DS12501	227,062	16
Cardiac fibroblasts	HCFaa-DS13480	234,383	21
Cardiac fibroblasts	HCFaa-DS13484	221,282	13
Cardiac myocytes	HCM-DS12589	210,319	11
Cardiac myocytes	HCM-DS12599	248,563	14
$CD3^+$ T cells *	CD3_CordBlood-DS17702	106,424	14
$CD3^+$ T cells *	CD3_CordBlood-DS17706	114,817	15
$CD3^+$ T cells *	CD3-DS11148	84,250	14
$CD3^+$ T cells *	CD3-DS16834	133,921	22
$CD3^+$ T cells *	CD3-DS17198	121,716	17
$CD3^+$ T cells *	CD3-DS17534	120,488	18
$CD34^+$ cells	CD34-DS11202	156,100	12
$CD34^+$ cells	CD34-DS11666	170,887	16
$CD34^+$ cells	CD34-DS12274	187,144	15
$CD34^+$ cells	CD34-DS12336	162,461	10
$CD34^+$ cells	CD34-DS12339	151,146	10
$CD34^+$ cells	CD34-DS12734	178,420	13
$CD34^+$ cells	CD34-DS12771	152,790	14
$CD34^+$ cells	CD34-DS12774	175,406	12
$CD34^+$ cells	CD34-DS12785	185,488	12
$CD34^+$ cells	CD34-DS13196	164,460	12
$CD34^+$ cells	CD34-DS13199	148,010	11
$CD34^+$ cells	CD34-DS14040	154,490	12
$CD34^+$ cells	CD34-DS14129	171,584	15
$CD34^+$ cells	CD34-DS14197	162,221	13
$CD34^+$ cells	CD34-DS14206	155,421	11
$CD34^+$ cells	CD34-DS16814	205,890	15

CD34$^+$ cells	CD34-DS17112	169,023	10
CD4$^+$ naïve T cells	CD4pos_N-DS14108	104,757	14
CD4$^+$ naïve T cells	CD4pos_N-DS15241	112,691	17
CD4$^+$ primary T cells *	CD4-DS15947	124,669	13
CD4$^+$ primary T cells *	CD4-DS16955	124,567	19
CD4$^+$ primary T cells *	CD4-DS17175	117,858	14
CD4$^+$ primary T cells *	CD4-DS17212	143,940	24
CD4$^+$ primary T cells *	CD4-DS17329	118,538	14
CD4$^+$ primary T cells *	CD4-DS17881	121,706	13
CD8$^+$ T cells	CD8-DS16012	124,099	26
CD8$^+$ T cells	CD8-DS16962	133,266	17
CD8$^+$ T cells	CD8-DS17203	124,572	23
CD8$^+$ T cells	CD8-DS17332	108,905	16
CD8$^+$ T cells	CD8-DS17885	114,186	16
Choroid plexus epithelial cells	HCPEpiC-DS12447	267,753	15
Choroid plexus epithelial cells	HCPEpiC-DS12457	236,411	20
Conjunctival fibroblast	HConF-DS11637	211,867	15
Conjunctival fibroblast	HConF-DS11642	199,405	8
Dermal fibroblasts	NHDF_Ad-DS12855	281,371	9
Dermal fibroblasts	NHDF_Ad-DS12863	288,809	9
Dermal fibroblasts	NHDF_Neo-DS11918	228,433	10
Dermal fibroblasts	NHDF_Neo-DS11923	240,920	13
Dermal microvascular endothelial cells	HMVEC_dAd-DS12952	131,768	8
Dermal microvascular endothelial cells	HMVEC_dAd-DS12957	160,720	7
Dermal microvascular endothelial cells	HMVEC_dBlNeo-DS13233	202,620	8
Dermal microvascular endothelial cells	HMVEC_dBlNeo-DS13242	214,283	8
Epidermal keratinocytes	NHEK-DS11474	184,655	12
Epidermal keratinocytes	NHEK-DS11476	192,267	14
Epidermal keratinocytes	wgEncodeOpenChromDnaseNhek	200,797	18
Esophageal epithelial cells	HEEpiC-DS12763	258,684	20
Esophageal epithelial cells	HEEpiC-DS12768	226,493	21
Fibroblasts	GM04503D-DS18637	254,114	10
Fibroblasts	GM04503D-DS18640	236,114	12
Fibroblasts	GM04504A-DS18973	241,248	10
Fibroblasts	GM04504A-DS18975	239,567	8
Gastric mucosa	Gastric_Mucosa-DS20260	225,013	16
Gastric mucosa	Gastric_Mucosa-DS20748	202,447	17
Gingival fibroblasts	HGF-DS11738	185,889	15
Gingival fibroblasts	HGF-DS11752	189,032	16
Gum tissue fibroblasts	AG09319-DS12286	184,998	12
Gum tissue fibroblasts	AG09319-DS12291	184,591	10
Heart tissue	Heart-DS20383	212,644	9
Iris pigment epithelial cells	HIPEpiC-DS12684	284,533	20
Iris pigment epithelial cells	HIPEpiC-DS12689	292,052	25
Lung fibroblasts	HPF-DS13380	214,583	16
Lung fibroblasts	HPF-DS13390	200,685	11
Lung fibroblasts	NHLF-DS12829	263,408	11
Lung fibroblasts	NHLF-DS12834	229,654	8
Lymphatic microvascular endothelial cells	HMVEC_dLyNeo-DS13146	195,084	9
Lymphatic microvascular endothelial cells	HMVEC_dLyNeo-DS13150	195,596	8
Lymphatic microvascular endothelial cells (lung derived)	HMVEC_LLy-DS13185	183,694	12
Lymphatic microvascular endothelial cells (lung derived)	HMVEC_LLy-DS13193	170,635	12
Mammary epithelial cells	HMEC-DS13921	184,269	18
Mammary epithelial cells	HMEC-DS8680	180,105	15
Mammary epithelial cells	vHMEC-DS18406	213,890	16
Mammary epithelial cells	vHMEC-DS18438	211,487	14
Mammary epithelial cells	wgEncodeOpenChromDnaseHmec	344,204	28
Mammary fibroblasts	HMF-DS13363	227,877	11
Mammary fibroblasts	HMF-DS13368	241,303	10
Marrow stromal cells	HS27a-DS16602	204,602	16
Marrow stromal cells	HS5-DS16597	226,005	8
Mesenchymal stem cells (H1 derived)	MSC-DS20514	278,237	19
Mesenchymal stem cells (H1 derived)	MSC-DS20518	227,074	15
Mesenchymal stem cells (H1 derived)	MSC-DS20671	210,267	10
Mesenchymal stem cells (H1 derived)	MSC-DS21042	228,391	13
Mesendoderm cultured cells (H1 derived)	Mesendoderm-DS18732	219,571	18
Mesendoderm cultured cells (H1 derived)	Mesendoderm-DS19310	258,507	21
Monocytes	CD14-DS16508	212,246	22

Monocytes	CD14-DS17215	154,784	18
Monocytes	CD14-DS17391	125,230	16
Monocytes	CD14-DS17889	140,861	17
Monocytes	CD14-DS18065	169,326	17
Neuronal progenitor cultured cells (H1 derived)	NPC-DS18739	139,124	6
Neuronal progenitor cultured cells (H1 derived)	NPC-DS20153	176,242	16
NK cells	CD56-DS16376	139,295	26
NK cells	CD56-DS17189	128,883	23
NK cells	CD56-DS17443	108,784	19
Non-pigment ciliary epithelial cells	HNPCEpiC-DS12467	269,225	17
Non-pigment ciliary epithelial cells	HNPCEpiC-DS12471	222,945	9
Ovary tissue	Ovary-DS20827	194,588	19
Pancreas tissue	Pancreas-DS20753	189,361	13
Pancreas tissue	Pancreas-DS20842	200,172	12
Periodontal ligament fibroblasts	HPdLF-DS13569	202,167	13
Periodontal ligament fibroblasts	HPdLF-DS13573	220,015	12
Pulmonary artery endothelial cells	HPAEC-DS12916	158,790	6
Pulmonary artery fibroblasts	HPAF-DS13411	240,676	14
Pulmonary artery fibroblasts	HPAF-DS13416	214,416	10
Renal endothelial cells	HRGEC-DS13705	182,281	11
Renal endothelial cells	HRGEC-DS13716	178,855	8
Renal epithelial cells	HRCE-DS10662	234,883	16
Renal epithelial cells	HRCE-DS10666	244,571	17
Renal epithelial cells	HRE-DS10631	228,830	15
Renal epithelial cells	HRE-DS10641	240,528	11
Renal proximal tubule epithelial cells	RPTEC-DS14061	215,927	13
Renal proximal tubule epithelial cells	RPTEC-DS14065	225,128	17
Retinal pigment epithelial cells	HRPEpiC-DS12568	256,447	12
Retinal pigment epithelial cells	HRPEpiC-DS12583	282,843	12
Skeletal muscle cells	HSMM_D-DS15538	310,296	18
Skeletal muscle cells	HSMM_D-DS15542	285,704	17
Skeletal muscle cells	HSMM-DS14426	287,942	14
Skeletal muscle cells	HSMM-DS14430	285,572	17
Skeletal muscle cells	Psoas_Muscle-DS20325	203,485	12
Skeletal muscle cells	SKMC-DS11939	265,175	15
Skeletal muscle cells	SKMC-DS11949	262,686	16
Skeletal muscle cells	wgEncodeOpenChromDnaseHsmm	205,571	18
Skeletal muscle cells	wgEncodeOpenChromDnaseHsmmt	223,138	32
Skin fibroblasts	AG10803-DS12374	232,609	12
Skin fibroblasts	AG10803-DS12384	220,125	9
Skin fibroblasts	BJ-DS10018	218,577	12
Skin fibroblasts	BJ-DS10081	210,687	11
Skin fibroblasts	HFF_MyC-DS15073	187,004	10
Skin fibroblasts	HFF_MyC-DS15079	269,783	16
Skin fibroblasts	HFF-DS15115	247,544	11
Skin fibroblasts	HFF-DS15119	228,514	10
Skin fibroblasts	Skin_Fibroblasts-DS18224	321,715	21
Skin fibroblasts	Skin_Fibroblasts-DS18229	289,323	15
Skin fibroblasts	Skin_Fibroblasts-DS18252	273,885	13
Skin fibroblasts	Skin_Fibroblasts-DS18256	261,980	13
Skin keratinocytes	Skin_Keratinocytes-DS18692	259,688	19
Skin keratinocytes	Skin_Keratinocytes-DS18695	248,115	17
Skin keratinocytes	Skin_Keratinocytes-DS18714	233,019	18
Skin keratinocytes	Skin_Keratinocytes-DS18718	243,192	17
Skin melanocytes	Skin_Melanocytes-DS18590	217,187	13
Skin melanocytes	Skin_Melanocytes-DS18601	237,348	11
Skin melanocytes	Skin_Melanocytes-DS18668	203,004	11
Skin melanocytes	Skin_Melanocytes-DS19662	179,179	11
Small airway epithelial cells	SAEC-DS10514	217,922	18
Small airway epithelial cells	SAEC-DS10518	246,080	20
Small bowel mucosa	Small_Bowel_Mucosa-DS20770	205,217	15
T_H1 cells	Adult_Th1	341,158	36
T_H1 cells	hTH1-DS17592	104,516	21
T_H1 cells	hTH1-DS17593	150,368	36
T_H1 cells	hTH1-DS18015	138,928	34
T_H1 cells	hTH1-DS7840	112,168	26
T_H1 cells	iTH1-DS18018	163,381	32
T_H17 cells	hTH17-DS11039	99,336	24

T_H2 cells	hTH2-DS17597	158,083	26
T_H2 cells	hTH2-DS18057	130,479	23
T_H2 cells	hTH2-DS7842	120,910	13
T_H2 cells	iTH2-DS17603	163,261	31
Toe fibroblasts	AG09309-DS12352	256,326	16
Toe fibroblasts	AG09309-DS12357	211,656	12
T_{REG} cells	hTR-DS14702	157,354	26
T_{REG} cells	hTR-DS17589	200,402	30
Trophoblast cultured cells (H1 derived)	Trophoblast-DS18736	156,571	7
Trophoblast cultured cells (H1 derived)	Trophoblast-DS19317	178,923	11
Umbilical vein endothelial cells (HUVEC)	HUVEC-DS10060	157,032	10
Umbilical vein endothelial cells (HUVEC)	HUVEC-DS13475	172,355	6
Umbilical vein endothelial cells (HUVEC)	wgEncodeOpenChromDnaseHuvec	190,575	14
Villous mesenchymal fibroblast cells	HVMF-DS13977	234,481	16
Villous mesenchymal fibroblast cells	HVMF-DS13981	221,750	14

Fetal adrenal tissue	fAdrenal-DS12528	239,260	16
Fetal adrenal tissue	fAdrenal-DS15123	237,417	13
Fetal adrenal tissue	fAdrenal-DS17319	188,785	6
Fetal adrenal tissue	fAdrenal-DS17677	171,942	12
Fetal adrenal tissue	fAdrenal-DS19395	204,599	11
Fetal adrenal tissue	fAdrenal-DS19583	227,942	12
Fetal adrenal tissue	fAdrenal-DS20343	248,414	22
Fetal brain tissue	fBrain-DS11872	224,908	21
Fetal brain tissue	fBrain-DS11877	233,453	21
Fetal brain tissue	fBrain-DS14464	242,866	21
Fetal brain tissue	fBrain-DS14717	254,590	6
Fetal brain tissue	fBrain-DS14718	237,507	7
Fetal brain tissue	fBrain-DS14803	217,868	17
Fetal brain tissue	fBrain-DS14815	221,266	14
Fetal brain tissue	fBrain-DS15453	244,347	15
Fetal brain tissue	fBrain-DS16302	212,268	12
Fetal brain tissue	fBrain-DS20221	269,189	6
Fetal brain tissue	fBrain-DS20226	235,312	19
Fetal brain tissue	fBrain-DS20231	221,164	17
Fetal brain tissue	fBrain-DS20780	254,310	17
Fetal fibroblasts	AG04449-DS12319	214,387	9
Fetal fibroblasts	AG04449-DS12329	212,307	13
Fetal heart tissue	fHeart-DS12531	225,000	6
Fetal heart tissue	fHeart-DS12810	271,123	9
Fetal heart tissue	fHeart-DS15643	208,559	6
Fetal heart tissue	fHeart-DS15839	269,385	11
Fetal heart tissue	fHeart-DS16018	228,562	4
Fetal heart tissue	fHeart-DS16146	235,849	6
Fetal heart tissue	fHeart-DS16500	245,587	6
Fetal heart tissue	fHeart-DS16582	247,095	8
Fetal heart tissue	fHeart-DS16621	233,123	7
Fetal heart tissue	fHeart-DS16819	278,526	10
Fetal heart tissue	fHeart-DS19427	278,026	13
Fetal heart tissue	fHeart-DS19431	259,866	8
Fetal kidney tissue	fKidney_L-DS16446	237,076	10
Fetal kidney tissue	fKidney_L-DS16579	261,475	10
Fetal kidney tissue	fKidney_L-DS16805	290,524	13
Fetal kidney tissue	fKidney_L-DS17140	227,089	9
Fetal kidney tissue	fKidney_L-DS18466	256,181	10
Fetal kidney tissue	fKidney_L-DS20920	312,502	11
Fetal kidney tissue	fKidney_L-DS20953	307,412	8
Fetal kidney tissue	fKidney_L-DS21344	267,940	11
Fetal kidney tissue	fKidney_R-DS15651	265,765	14
Fetal kidney tissue	fKidney_R-DS16441	254,362	8
Fetal kidney tissue	fKidney_R-DS16801	292,195	10
Fetal kidney tissue	fKidney_R-DS17144	235,190	7
Fetal kidney tissue	fKidney_R-DS18463	243,750	12
Fetal kidney tissue	fKidney_R-DS20917	283,050	11
Fetal kidney tissue	fKidney_R-DS20951	277,275	10
Fetal kidney tissue	fKidney_R-DS21044	216,284	6
Fetal kidney tissue	fKidney_R-DS21340	270,388	14

Fetal kidney tissue	fKidney-DS10986	266,759	7
Fetal kidney tissue	fKidney-DS12635	225,491	7
Fetal kidney tissue	fKidney-DS16139	281,020	11
Fetal kidney tissue	fKidney-DS16837	241,597	15
Fetal kidney tissue	fKidney-DS17068	235,705	10
Fetal kidney tissue	fKidney-DS17522	289,955	13
Fetal kidney tissue	fKidney-DS17753	219,447	8
Fetal kidney tissue	fKidney-DS20564	246,375	7
Fetal kidney tissue	fKidney-DS20786	275,125	6
Fetal kidney tissue	fKidney-DS20987	227,064	8
Fetal kidney tissue	fKidney-DS20988	259,876	9
Fetal kidney tissue	fKidney-DS21096	311,948	15
Fetal large intestine tissue	fIntestine_Lg-DS16027	199,028	14
Fetal large intestine tissue	fIntestine_Lg-DS16164	217,553	18
Fetal large intestine tissue	fIntestine_Lg-DS16563	229,851	19
Fetal large intestine tissue	fIntestine_Lg-DS17094	229,118	23
Fetal large intestine tissue	fIntestine_Lg-DS17157	216,931	15
Fetal large intestine tissue	fIntestine_Lg-DS17313	114,101	11
Fetal large intestine tissue	fIntestine_Lg-DS17422	193,211	15
Fetal large intestine tissue	fIntestine_Lg-DS17462	222,892	19
Fetal large intestine tissue	fIntestine_Lg-DS17502	111,613	11
Fetal large intestine tissue	fIntestine_Lg-DS17647	237,118	19
Fetal large intestine tissue	fIntestine_Lg-DS17748	200,602	15
Fetal large intestine tissue	fIntestine_Lg-DS17785	216,036	17
Fetal large intestine tissue	fIntestine_Lg-DS17841	358,040	32
Fetal large intestine tissue	fIntestine_Lg-DS17990	245,075	16
Fetal large intestine tissue	fIntestine_Lg-DS18499	228,192	20
Fetal lung fibroblasts	AG04450-DS12255	201,391	10
Fetal lung fibroblasts	AG04450-DS12270	192,559	12
Fetal lung fibroblasts	WI_38_TAM-DS14323	258,089	14
Fetal lung fibroblasts	WI_38_TAM-DS14328	212,246	11
Fetal lung fibroblasts	WI_38-DS14315	212,805	10
Fetal lung fibroblasts	WI_38-DS14320	188,762	9
Fetal lung tissue	fLung_L-DS15637	250,704	14
Fetal lung tissue	fLung_L-DS16570	249,920	17
Fetal lung tissue	fLung_L-DS17105	249,830	18
Fetal lung tissue	fLung_L-DS17154	272,229	18
Fetal lung tissue	fLung_L-DS17464	251,021	16
Fetal lung tissue	fLung_L-DS17674	256,668	19
Fetal lung tissue	fLung_L-DS17739	231,938	13
Fetal lung tissue	fLung_L-DS17835	202,511	12
Fetal lung tissue	fLung_L-DS17959	246,599	17
Fetal lung tissue	fLung_L-DS18170	298,414	18
Fetal lung tissue	fLung_L-DS18421	262,423	17
Fetal lung tissue	fLung_L-DS18487	278,850	18
Fetal lung tissue	fLung_L-DS21334	244,734	19
Fetal lung tissue	fLung_R-DS15632	224,177	18
Fetal lung tissue	fLung_R-DS16566	241,400	20
Fetal lung tissue	fLung_R-DS16790	270,372	21
Fetal lung tissue	fLung_R-DS17101	252,769	16
Fetal lung tissue	fLung_R-DS17162	236,762	15
Fetal lung tissue	fLung_R-DS17670	288,965	15
Fetal lung tissue	fLung_R-DS17831	285,265	20
Fetal lung tissue	fLung_R-DS17954	264,896	16
Fetal lung tissue	fLung_R-DS18418	263,746	18
Fetal lung tissue	fLung_R-DS18492	276,689	15
Fetal lung tissue	fLung_R-DS21328	262,453	14
Fetal lung tissue	fLung-DS12646	208,762	13
Fetal lung tissue	fLung-DS12817	287,861	18
Fetal lung tissue	fLung-DS13507	264,039	21
Fetal lung tissue	fLung-DS13985	260,023	23
Fetal lung tissue	fLung-DS14666	221,321	12
Fetal lung tissue	fLung-DS14724	270,963	16
Fetal lung tissue	fLung-DS14751	263,458	16
Fetal lung tissue	fLung-DS14809	210,774	14
Fetal lung tissue	fLung-DS14820	234,213	16
Fetal lung tissue	fLung-DS15227	228,533	18
Fetal lung tissue	fLung-DS15461	264,761	20

Fetal lung tissue	fLung-DS15573	234,527	10
Fetal muscle tissue	fMuscle_arm-DS17432	262,089	17
Fetal muscle tissue	fMuscle_arm-DS17765	406,263	21
Fetal muscle tissue	fMuscle_arm-DS17825	266,958	12
Fetal muscle tissue	fMuscle_arm-DS17848	267,476	15
Fetal muscle tissue	fMuscle_arm-DS18080	306,683	19
Fetal muscle tissue	fMuscle_arm-DS18176	238,043	18
Fetal muscle tissue	fMuscle_arm-DS18379	192,450	11
Fetal muscle tissue	fMuscle_arm-DS18452	239,163	16
Fetal muscle tissue	fMuscle_arm-DS18473	236,430	15
Fetal muscle tissue	fMuscle_arm-DS18559	238,326	16
Fetal muscle tissue	fMuscle_arm-DS18992	199,180	17
Fetal muscle tissue	fMuscle_arm-DS19051	205,604	15
Fetal muscle tissue	fMuscle_arm-DS19053	224,777	14
Fetal muscle tissue	fMuscle_arm-DS19270	254,472	18
Fetal muscle tissue	fMuscle_arm-DS19295	261,040	16
Fetal muscle tissue	fMuscle_arm-DS19380	262,039	12
Fetal muscle tissue	fMuscle_arm-DS19439	188,681	14
Fetal muscle tissue	fMuscle_arm-DS19646	224,368	13
Fetal muscle tissue	fMuscle_back-DS17767	304,941	19
Fetal muscle tissue	fMuscle_back-DS17850	286,323	15
Fetal muscle tissue	fMuscle_back-DS18083	315,067	19
Fetal muscle tissue	fMuscle_back-DS18377	223,390	13
Fetal muscle tissue	fMuscle_back-DS18454	257,441	13
Fetal muscle tissue	fMuscle_back-DS18468	258,750	14
Fetal muscle tissue	fMuscle_back-DS18842	240,033	14
Fetal muscle tissue	fMuscle_back-DS19117	206,932	16
Fetal muscle tissue	fMuscle_back-DS19384	270,166	9
Fetal muscle tissue	fMuscle_back-DS19441	247,335	13
Fetal muscle tissue	fMuscle_back-DS19648	318,211	13
Fetal muscle tissue	fMuscle_back-DS20244	243,554	12
Fetal muscle tissue	fMuscle_back-DS20789	250,916	14
Fetal muscle tissue	fMuscle_back-DS21048	235,973	12
Fetal muscle tissue	fMuscle_leg-DS17429	249,673	15
Fetal muscle tissue	fMuscle_leg-DS18386	251,317	11
Fetal muscle tissue	fMuscle_leg-DS18456	236,671	12
Fetal muscle tissue	fMuscle_leg-DS18471	259,785	14
Fetal muscle tissue	fMuscle_leg-DS18844	181,791	9
Fetal muscle tissue	fMuscle_leg-DS19115	244,480	14
Fetal muscle tissue	fMuscle_leg-DS19158	263,781	17
Fetal muscle tissue	fMuscle_leg-DS19272	277,079	13
Fetal muscle tissue	fMuscle_leg-DS19291	270,313	14
Fetal muscle tissue	fMuscle_leg-DS19382	222,200	10
Fetal muscle tissue	fMuscle_leg-DS19436	270,484	15
Fetal muscle tissue	fMuscle_leg-DS19643	264,525	14
Fetal muscle tissue	fMuscle_leg-DS20239	288,372	12
Fetal muscle tissue	fMuscle_leg-DS20797	260,053	14
Fetal muscle tissue	fMuscle_lower_limb-DS18174	332,489	24
Fetal muscle tissue	fMuscle_trunk-DS17827	270,215	16
Fetal muscle tissue	fMuscle_trunk-DS20242	261,643	17
Fetal muscle tissue	fMuscle_trunk-DS20544	242,440	15
Fetal muscle tissue	fMuscle_upper_back-DS19283	218,423	16
Fetal muscle tissue	fMuscle_upper_limb_sk-DS17661	231,931	17
Fetal muscle tissue	fMuscle_upper_trunk-DS17664	276,446	19
Fetal ovary	fOvary-DS17445	175,291	17
Fetal placenta	fPlacenta-DS17639	287,200	27
Fetal placenta	fPlacenta-DS17744	228,065	20
Fetal placenta	fPlacenta-DS19391	240,708	26
Fetal placenta	fPlacenta-DS20346	225,737	24
Fetal placenta	fPlacenta-DS20793	257,034	27
Fetal placenta	fPlacenta-DS21111	277,837	21
Fetal renal cortex	fKidney_renal_cortex_L-DS17550	260,167	11
Fetal renal cortex	fKidney_renal_cortex_L-DS18542	269,183	9
Fetal renal cortex	fKidney_renal_cortex_L-DS18931	220,018	10
Fetal renal cortex	fKidney_renal_cortex_L-DS19257	301,966	11
Fetal renal cortex	fKidney_renal_cortex_R-DS17545	253,847	11
Fetal renal cortex	fKidney_renal_cortex_R-DS18928	246,280	8
Fetal renal cortex	fKidney_renal_cortex_R-DS19254	282,614	9

Fetal renal cortex	fKidney_renal_cortex-DS17307	175,158	10
Fetal renal cortex	fKidney_renal_cortex-DS17387	270,509	9
Fetal renal cortex	fKidney_renal_cortex-DS17455	319,483	10
Fetal renal cortex	fKidney_renal_cortex-DS17756	220,328	8
Fetal renal cortex	fKidney_renal_cortex-DS17804	274,440	7
Fetal renal cortex	fKidney_renal_cortex-DS18428	247,676	9
Fetal renal cortex	fKidney_renal_cortex-DS19388	239,419	10
Fetal renal cortex	fKidney_renal_cortex-DS20018	240,500	7
Fetal renal cortex	fKidney_renal_cortex-DS20024	263,619	8
Fetal renal cortex	fKidney_renal_cortex-DS20445	294,348	9
Fetal renal cortex	fKidney_renal_cortex-DS20568	298,780	10
Fetal renal pelvis	fKidney_renal_pelvis_L-DS17553	253,084	7
Fetal renal pelvis	fKidney_renal_pelvis_L-DS18666	240,616	8
Fetal renal pelvis	fKidney_renal_pelvis_L-DS18964	232,285	10
Fetal renal pelvis	fKidney_renal_pelvis_L-DS19238	270,193	8
Fetal renal pelvis	fKidney_renal_pelvis_R-DS17548	243,133	5
Fetal renal pelvis	fKidney_renal_pelvis_R-DS18663	282,071	10
Fetal renal pelvis	fKidney_renal_pelvis_R-DS18961	239,379	7
Fetal renal pelvis	fKidney_renal_pelvis_R-DS19235	246,156	9
Fetal renal pelvis	fKidney_renal_pelvis-DS17381	288,643	9
Fetal renal pelvis	fKidney_renal_pelvis-DS17451	261,684	13
Fetal renal pelvis	fKidney_renal_pelvis-DS17760	260,905	12
Fetal renal pelvis	fKidney_renal_pelvis-DS18088	169,948	6
Fetal renal pelvis	fKidney_renal_pelvis-DS18431	234,406	11
Fetal renal pelvis	fKidney_renal_pelvis-DS19386	258,071	8
Fetal renal pelvis	fKidney_renal_pelvis-DS20022	286,362	11
Fetal renal pelvis	fKidney_renal_pelvis-DS20027	233,092	7
Fetal renal pelvis	fKidney_renal_pelvis-DS20448	322,488	11
Fetal renal pelvis	fKidney_renal_pelvis-DS20570	297,997	13
Fetal skin	fSkin-DS10987	220,690	9
Fetal skin fibroblasts	fSkin_fibro_abdomen-DS19558	218,329	8
Fetal skin fibroblasts	fSkin_fibro_abdomen-DS19561	236,795	7
Fetal skin fibroblasts	fSkin_fibro_back-DS19174	219,997	15
Fetal skin fibroblasts	fSkin_fibro_back-DS19233	225,696	15
Fetal skin fibroblasts	fSkin_fibro_bicep_L-DS19857	222,207	9
Fetal skin fibroblasts	fSkin_fibro_bicep_L-DS19867	217,057	10
Fetal skin fibroblasts	fSkin_fibro_bicep_R-DS19745	216,446	8
Fetal skin fibroblasts	fSkin_fibro_bicep_R-DS19761	222,332	8
Fetal skin fibroblasts	fSkin_fibro_leg_L_quad-DS20046	247,329	11
Fetal skin fibroblasts	fSkin_fibro_leg_L_quad-DS20056	243,893	10
Fetal skin fibroblasts	fSkin_fibro_leg_R_quad-DS19943	211,007	10
Fetal skin fibroblasts	fSkin_fibro_leg_R_quad-DS19948	235,371	10
Fetal skin fibroblasts	fSkin_fibro_scalp-DS19444	215,217	12
Fetal skin fibroblasts	fSkin_fibro_scalp-DS19449	219,626	11
Fetal skin fibroblasts	fSkin_fibro_upper_back-DS19696	228,230	14
Fetal skin fibroblasts	fSkin_fibro_upper_back-DS19706	263,171	11
Fetal small intestine tissue	fIntestine_Sm-DS16559	241,735	18
Fetal small intestine tissue	fIntestine_Sm-DS16712	178,934	16
Fetal small intestine tissue	fIntestine_Sm-DS16822	250,946	16
Fetal small intestine tissue	fIntestine_Sm-DS16975	222,123	16
Fetal small intestine tissue	fIntestine_Sm-DS17092	223,170	19
Fetal small intestine tissue	fIntestine_Sm-DS17150	210,436	14
Fetal small intestine tissue	fIntestine_Sm-DS17317	196,775	23
Fetal small intestine tissue	fIntestine_Sm-DS17425	121,891	12
Fetal small intestine tissue	fIntestine_Sm-DS17643	228,567	14
Fetal small intestine tissue	fIntestine_Sm-DS17763	228,689	23
Fetal small intestine tissue	fIntestine_Sm-DS17808	242,145	18
Fetal small intestine tissue	fIntestine_Sm-DS17844	237,577	14
Fetal small intestine tissue	fIntestine_Sm-DS18495	217,807	19
Fetal spinal cord	fSpinal_cord-DS18501	292,271	5
Fetal spinal cord	fSpinal_cord-DS19260	221,443	10
Fetal spinal cord	fSpinal_cord-DS20351	262,720	16
Fetal spinal cord	fSpinal_cord-DS20530	245,437	12
Fetal spinal cord	fSpinal_cord-DS20956	215,266	9
Fetal spleen	fSpleen-DS17448	227,282	16
Fetal stomach	fStomach-DS16530	206,921	16
Fetal stomach	fStomach-DS17172	217,031	13
Fetal stomach	fStomach-DS17325	142,757	11

Fetal stomach	fStomach-DS17659	223,240	16
Fetal stomach	fStomach-DS17750	177,536	13
Fetal stomach	fStomach-DS17878	270,050	19
Fetal stomach	fStomach-DS17963	220,227	16
Fetal stomach	fStomach-DS18389	192,936	15
Fetal stomach	fStomach-DS18821	215,802	11
Fetal stomach	fStomach-DS19933	241,276	21
Fetal stomach	fStomach-DS20079	243,537	11
Fetal stomach	fStomach-DS20349	233,102	14
Fetal stomach	fStomach-DS20546	236,515	20
Fetal stomach	fStomach-DS20791	211,415	14
Fetal testes	fTestes-DS18942	226,342	10
Fetal testes	fTestes-DS20170	231,064	11
Fetal thymus	fThymus-DS16490	171,022	43
Fetal thymus	fThymus-DS16841	150,724	28
Fetal thymus	fThymus-DS17323	144,746	38
Fetal thymus	fThymus-DS17474	148,201	40
Fetal thymus	fThymus-DS17875	145,658	41
Fetal thymus	fThymus-DS17876	190,176	46
Fetal thymus	fThymus-DS18382	203,865	43
Fetal thymus	fThymus-DS19287	196,719	8
Fetal thymus	fThymus-DS19675	164,434	58
Fetal thymus	fThymus-DS20335	144,632	49
Fetal thymus	fThymus-DS20341	153,966	41

A549	A549-DS14285	173,554	13
A549	A549-DS14289	153,968	7
A549	wgEncodeOpenChromDnaseA549	160,688	9
BE2C	BE2_C-DS14625	218,560	8
BE2C	BE2_C-DS14635	220,932	12
CACO2	CACO2-DS8235	156,653	19
CACO2	CACO2-DS8416	140,069	18
CMK	CMK-DS12393	167,379	4
HCT116	HCT116-DS13547	144,714	14
HCT116	HCT116-DS13551	144,611	13
HEK293T	HEK293T-DS13691	80,885	4
HEK293T	HEK293T-DS13696	95,566	10
HELA	Hela-DS10011	159,166	15
HELA	Hela-DS8200	171,190	13
HELA	wgEncodeOpenChromDnaseHelas3	181,921	19
HEPG2	HEPG2-DS7764	118,570	10
HEPG2	HEPG2-DS7768	114,100	8
HEPG2	wgEncodeOpenChromDnaseHepg2	214,138	17
HESC	H1_P18-DS18873	223,271	27
HESC	H1_P18-DS19100	153,095	16
HESC	H7_hESC_T14-DS11814	163,882	7
HESC	H7_hESC_T14-DS12147	181,918	12
HESC	H7_hESC_T2-DS14732	208,630	8
HESC	H7_hESC_T5-DS11953	231,087	15
HESC	H7_hESC_T5-DS15665	263,665	18
HESC	H7_hESC_T9-DS15809	245,145	13
HESC	H9_P42-DS18517	216,783	17
HESC	H9_P42-DS18522	183,643	17
HESC	HESC-DS10167	192,966	23
HESC	hESCT0-DS11909	326,539	25
HESC	hESCT0-DS13133	265,127	23
HESC	wgEncodeOpenChromDnaseH1hesc	232,751	33
HL60	HL60-DS11733	178,032	20
HL60	HL60-DS11809	199,270	17
IMR90	IMR90-DS11759	194,623	16
IMR90	IMR90-DS11764	189,784	17
IMR90	IMR90-DS13219	253,026	14
IMR90	IMR90-DS13229	220,322	16
IPS cells	iPS_19_11-DS15153	243,074	24
IPS cells	iPS_19_7-DS15148	215,493	20
IPS cells	iPS_4_7-DS15169	219,356	23
IPS cells	iPS_6_9-DS15164	220,747	24

JURKAT	Jurkat-DS10681	152,255	28
JURKAT	Jurkat-DS12659	194,089	34
K562	K562-DS13204	210,649	20
K562	K562-DS13209	181,217	18
K562	K562-DS13277	178,134	15
K562	K562-DS13282	181,433	10
K562	K562-DS13287	203,857	12
K562	K562-DS13310	164,618	22
K562	K562-DS13906	172,247	15
K562	K562-DS14211	187,634	21
K562	K562-DS14216	183,276	18
K562	K562-DS14245	178,075	16
K562	K562-DS14250	183,028	16
K562	K562-DS14274	176,224	16
K562	K562-DS14279	194,682	17
K562	K562-DS15309	207,854	21
K562	K562-DS15358	191,890	12
K562	K562-DS15363	202,756	9
K562	K562-DS16924	187,807	19
K562	K562-DS16934	183,894	17
K562	K562-DS9764	181,544	26
K562	K562-DS9767	181,443	17
K562	wgEncodeOpenChromDnaseK562	153,438	14
LCL	GM06990-DS7748	121,937	20
LCL	GM06990-DS7784	118,460	15
LCL	GM12864-DS12431	173,730	28
LCL	GM12865-DS12436	179,926	24
LCL	GM12865-DS12442	186,974	33
LCL	GM12878-DS10671	150,916	20
LCL	GM12878-DS9432	150,282	22
LCL	wgEncodeOpenChromDnaseGm12878	168,844	24
LHCNM2	LHCN_M2_D4-DS20534	271,246	17
LHCNM2	LHCN_M2_D4-DS20647	270,156	18
LHCNM2	LHCN_M2-DS20485	244,218	15
LHCNM2	LHCN_M2-DS20548	241,195	14
LNCAP	LNCap-DS14680	232,792	18
LNCAP	LNCap-DS14684	219,666	22
LNCAP	wgEncodeOpenChromDnaseLncap	242,546	26
M059J	M059J-DS20493	273,845	14
M059J	M059J-DS20497	269,122	16
MCF7	MCF7_ER-DS18025	284,516	19
MCF7	MCF7_ER-DS18271	268,203	19
MCF7	MCF7-DS12619	215,829	14
MCF7	MCF7-DS18021	299,781	22
MCF7	MCF7-DS18267	254,492	18
MCF7	MCF7-DS9445	160,082	10
MCF7	wgEncodeOpenChromDnaseMcf7	181,064	14
NB4	NB4-DS12538	170,045	13
NB4	NB4-DS12543	180,983	13
NT2	NT2_D1-DS14564	184,600	11
NT2	NT2_D1-DS14575	228,165	14
PANC1	PANC1-DS9873	150,811	6
PANC1	PANC1-DS9955	151,327	8
PrEC	PrEC-DS12088	200,143	20
PrEC	PrEC-DS12098	209,654	20
RPMI7951	RPMI_7951-DS20904	207,826	6
RPMI7951	RPMI_7951-DS20909	212,669	8
SKNMC	SK_N_MC-DS14408	182,372	11
SKNMC	SK_N_MC-DS14413	187,234	10
SKNSH	SKNSH-DS8476	147,479	6
SKNSH	SKNSH-DS8482	118,678	4
T47D	T_47D-DS19790	185,571	12
T47D	T_47D-DS19794	188,392	14
WERIRB	WERI_Rb1-DS13670	226,821	15
WERIRB	WERI_Rb1-DS13681	228,592	16

* Data sets were excluded from downstream analysis (see **Methods**).

** *PTPN2* locus (extended to 140 kb): chr18: 12,760,001 - 12,900,000 (hg19).

Table S3. DNase hypersensitivity sites (DHS) in *PTPN2* locus in primary cell types, fetal tissues and cell lines; ordered by number of DHS in *PTPN2* locus.

Cell type or tissue	Frequency (no. of data sets)	Average no. of DHS genome-wide	Average no. of DHS in *PTPN2* locus **	DHS overlapping with *PTPN2* SNPs
T_H1 cells	6	168,420	31	12
T_{REG} cells	2	178,878	28	4
T_H17 cells	1	99,336	24	3
T_H2 cells	4	143,183	23	5
NK cells	3	125,654	23	6
Iris pigment epithelial cells	2	288,293	23	2
Brain vascular smooth muscle cells	2	207,986	22	2
Brain vascular pericytes	1	264,939	21	2
Bronchial epithelial cells (BEC)	2	199,006	21	1
Esophageal epithelial cells	2	242,589	21	1
$CD8^+$ T cells	5	121,006	20	6
Mesendoderm cultured cells (H1 derived)	2	239,039	20	4
Amniotic epithelial cells	2	256,238	19	2
Ovary tissue	1	194,588	19	1
Small airway epithelial cells	2	232,001	19	1
Mammary epithelial cells	5	226,791	18	8
Monocytes	5	160,489	18	3
Skin keratinocytes	4	246,004	18	1
Skeletal muscle cells	9	258,841	18	9
Choroid plexus epithelial cells	2	252,082	18	2
$CD3^+$ T cells *	6	113,603	17	5
Gastric mucosa	2	213,730	17	2
$CD4^+$ primary T cells *	6	125,213	16	5
Cardiac fibroblasts	4	224,800	16	5
$CD4^+$ naïve T cells	2	108,724	16	4
B cells	6	140,422	16	2
Gingival fibroblasts	2	187,461	16	2
Renal proximal tubule epithelial cells	2	220,528	15	3
Villous mesenchymal fibroblast cells	2	228,116	15	2
Small bowel mucosa	1	205,217	15	1
Renal epithelial cells	4	237,203	15	1
Epidermal keratinocytes	3	192,573	15	2
Mesenchymal stem cells (H1 derived)	4	235,992	14	3
Toe fibroblasts	2	233,991	14	1
Astrocytes	8	230,892	14	4
Non-pigment ciliary epithelial cells	2	246,085	13	3
Skin fibroblasts	12	246,812	13	4
$CD34^+$ cells	17	167,702	13	2
Cardiac myocytes	2	229,441	13	2
Pancreas tissue	2	194,767	13	2
Periodontal ligament fibroblasts	2	211,091	13	2
Pulmonary artery fibroblasts	2	227,546	12	2
Lymphatic microvascular endothelial cells (lung derived)	2	177,165	12	1
Marrow stromal cells	2	215,304	12	1
Retinal pigment epithelial cells	2	269,645	12	1
Lung fibroblasts	4	227,083	12	4
Skin melanocytes	4	209,180	12	3
Conjunctival fibroblast	2	205,636	12	1
Aortic adventitial fibroblasts	2	219,329	11	2
Gum tissue fibroblasts	2	184,795	11	2
Brain microvascular endothelial cells	2	236,353	11	1
Neuronal progenitor cultured cells (H1 derived)	2	157,683	11	1
Mammary fibroblasts	2	234,590	11	1
Dermal fibroblasts	4	259,883	10	1
Umbilical vein endothelial cells (HUVEC)	3	173,321	10	3
Fibroblasts	4	242,761	10	1

Blood microvascular endothelial cells	6	186,340	10	1
Renal endothelial cells	2	180,568	10	1
Heart tissue	1	212,644	9	1
Trophoblast cultured cells (H1 derived)	2	167,747	9	1
Lymphatic microvascular endothelial cells	2	195,340	9	1
Dermal microvascular endothelial cells	4	177,348	8	1
Blood microvascular endothelial cells (lung derived)	2	207,430	7	1
Pulmonary artery endothelial cells	1	158,790	6	1
Fetal thymus	11	164,922	40	12
Fetal placenta	6	252,764	24	8
Fetal large intestine tissue	15	214,624	18	7
Fetal small intestine tissue	13	215,446	17	6
Fetal ovary	1	175,291	17	4
Fetal lung tissue	36	253,127	17	4
Fetal spleen	1	227,282	16	2
Fetal stomach	14	216,596	15	3
Fetal brain tissue	13	236,081	15	2
Fetal muscle tissue	53	254,853	15	7
Fetal adrenal tissue	7	216,908	13	2
Fetal lung fibroblasts	6	210,975	11	2
Fetal fibroblasts	2	213,347	11	1
Fetal skin fibroblasts	16	227,669	11	1
Fetal testes	2	228,703	11	2
Fetal spinal cord	5	247,427	10	2
Fetal kidney tissue	29	261,339	10	5
Fetal renal cortex	18	259,908	9	4
Fetal renal pelvis	18	256,695	9	3
Fetal skin	1	220,690	9	1
Fetal heart tissue	12	248,392	8	2
JURKAT	2	173,172	31	4
LCL	8	156,384	23	6
IPS cells	4	224,668	23	7
LNCAP	3	231,668	22	6
PrEC	2	204,899	20	3
HL60	2	188,651	19	4
CACO2	2	148,361	19	3
HESC	14	220,607	18	9
K562	21	185,033	17	6
MCF7	7	237,710	17	3
LHCNM2	4	256,704	16	3
IMR90	4	214,439	16	2
HELA	3	170,759	16	2
WERIRB	2	227,707	16	1
M059J	2	271,484	15	1
HCT116	2	144,663	14	1
T47D	2	186,982	13	3
NB4	2	175,514	13	1
NT2	2	206,383	13	2
HEPG2	3	148,936	12	2
SKNMC	2	184,803	11	1
BE2C	2	219,746	10	1
A549	3	162,737	10	2
HEK293T	2	88,226	7	2
PANC1	2	151,069	7	1
RPMI7951	2	210,248	7	1
SKNSH	2	133,079	5	1
CMK	1	167,379	4	1

* Data sets were excluded from downstream analysis (see **Methods**).

** *PTPN2* locus (extended to 140 kb): chr18: 12,760,001 - 12,900,000 (hg19).

Unedited and uncropped Gels and Blots

Full unedited blot for Figure 13A

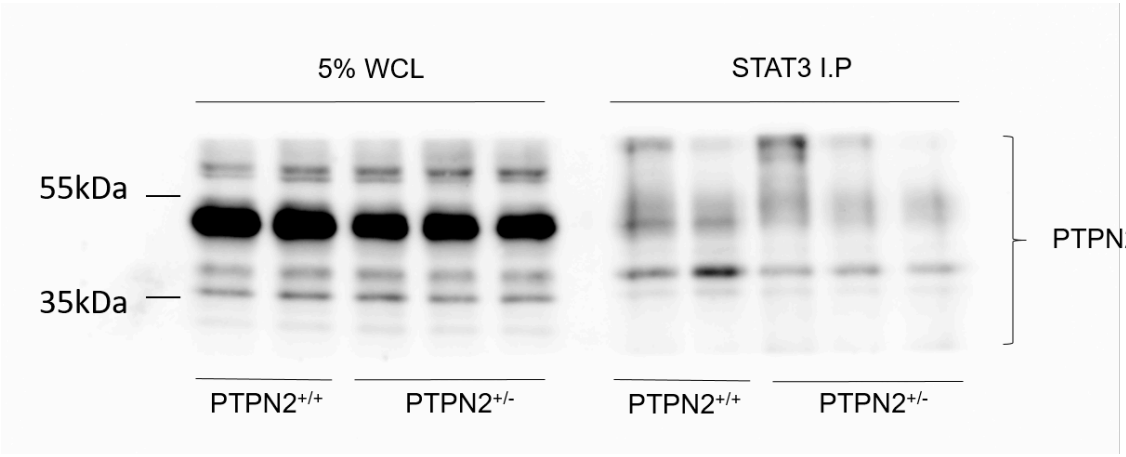

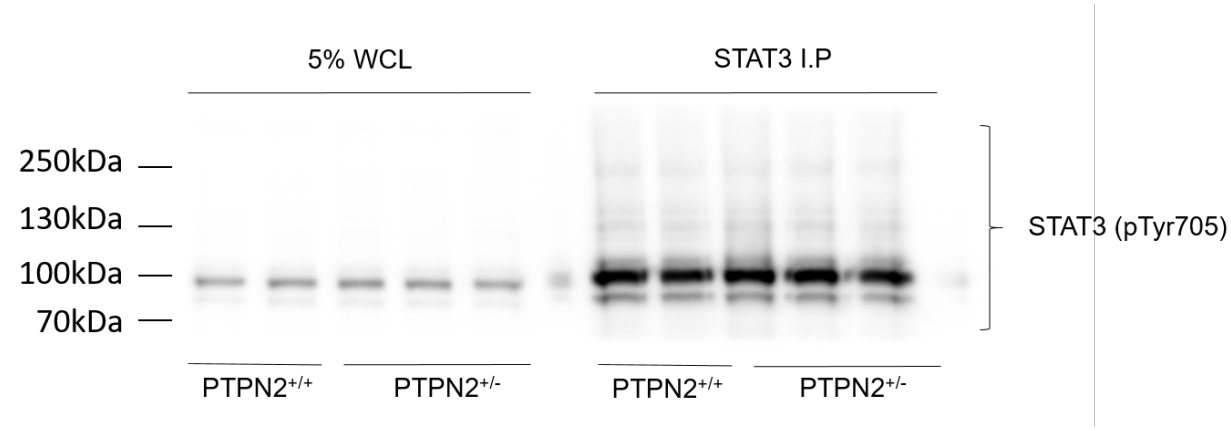

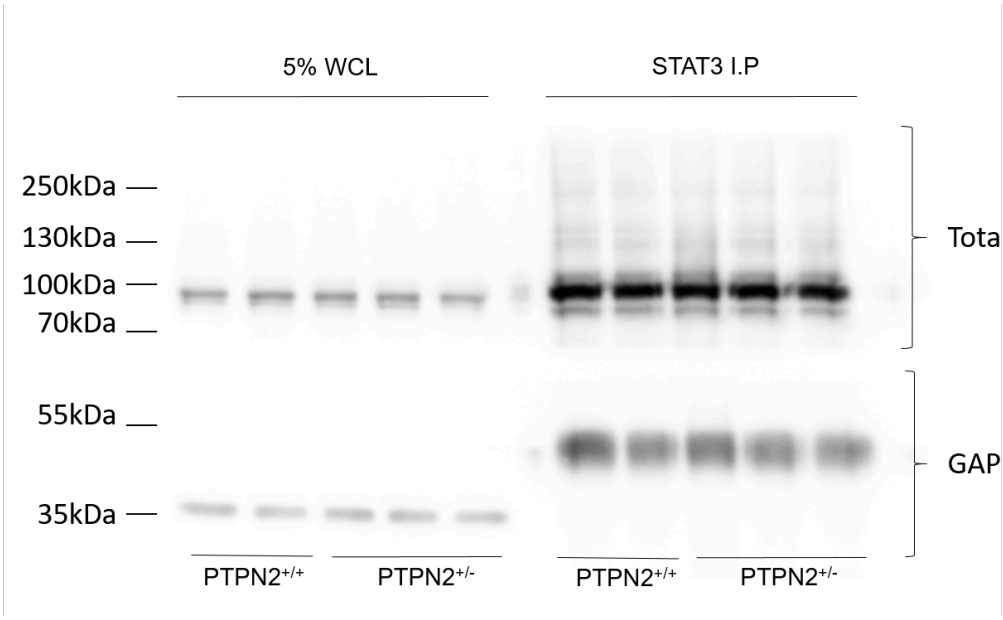

Full unedited blot for Figure 13B

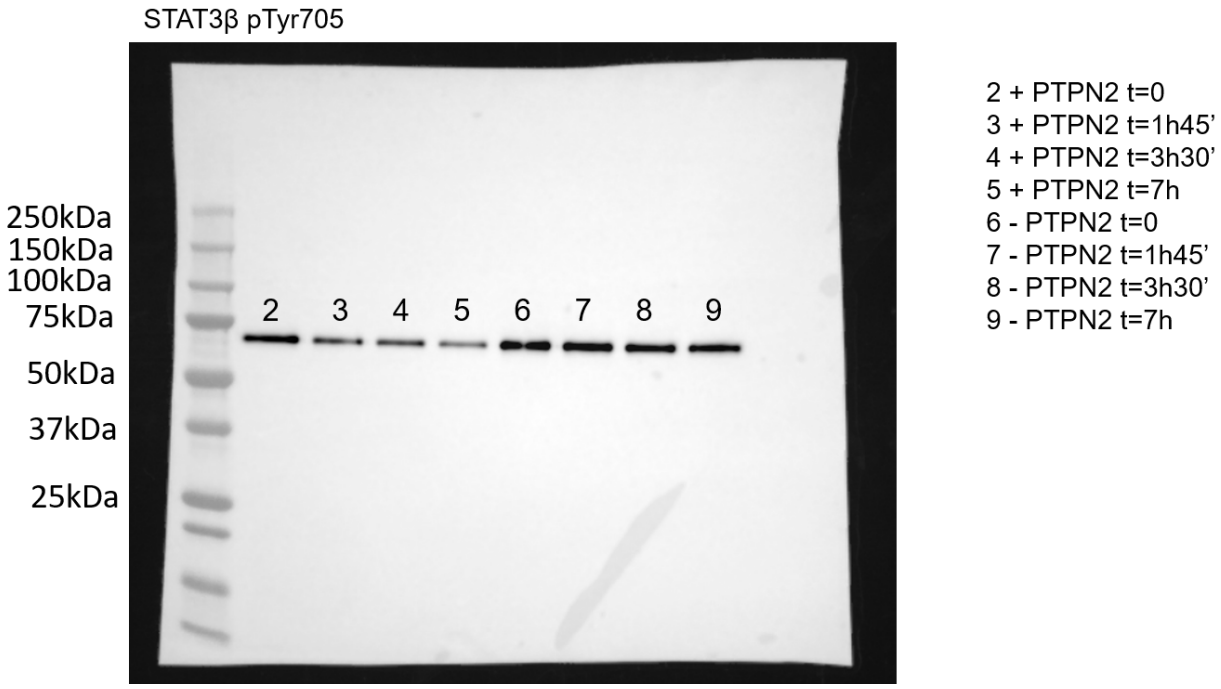

Full unedited gel for Figure 13C